Faisal, AAH, Mokif, LA, Hassan, WH, AlZubaidi, R, Al Marri, S, Hashim, K, Khan, MA and Alsareji, OJ

Continuous and funnel-gate configurations of a permeable reactive barrier for reclamation of groundwater laden with tetracycline: experimental and simulation approaches

scientific reports

Check for updates

OPEN

Continuous and funnel-gate configurations of a permeable reactive barrier for reclamation of groundwater laden with tetracycline: experimental and simulation approaches

Ayad A.H. Faisal[1]✉, Layla Abdulkareem Mokif[2], Waqed H. Hassan[3,4], Radhi AlZubaidi[5], Saeed Al Marri[6], Khalid Hashim[2,7]✉, Mohammad Amir Khan[8] & Osamah J. Alsareji[9]✉

The current study investigates removing tetracycline from water using batch, column, and tank experiments with statistical modelling using ANN for continuous tests. An artificial neural network (ANN) using the Levenberg-Marquardt back-propagation (LMA) training algorithm is constructed to compare the effectiveness of Tetracycline removal from aqueous solution using the sorption technique with prepared adsorbent. Several characterization analyses XRD, FT-IR, and SEM are employed for prepared Brownmillerite ($Ca_2Fe_2O_5$)–Na alginate beads. The operating conditions of batch tests involved, contact time (0.1–3 h), initial of tetracycline (C_o) of (100–250 mg/L), pH (3–12), agitation speed (50–250) rpm and dosage of adsorbent (0.2–1.2 g/50 mL). The outcomes of experiments have demonstrated that the optimum conditions for the batch test to achieve the maximum adsorbent capacity (q_{max} =7.845 mg/g) are achieved at pH 7, contact time 1.5 h, adsorbent dose 1.2 g/50 mL, agitation speed of 200 rpm, and initial concentration of TC 100 mg/L. Minimum mean square error (MSE) values of 7.09E-04 for 30 hidden neurons and 0.0029 for 59 hidden neurons in the 1D and 2D systems are accomplished, respectively. The artificial neural network model has exhibited excellent performance with correlation coefficients exceeding 0.980 for the operating variables, demonstrating its accuracy and effectiveness in predicting the experimental outcomes. According to sensitivity analysis, the influential parameter in the column test (1D) is the flow rate (mL/min), with a relative importance of 32.769%. However, in the tank test (2D), time (day) is signified as an influential parameter with a relative importance of 31.207%.

Keywords Adsorption, Artificial neural network, Brownmillerite compounds, Groundwater, Nanomaterial, Permeable reactive barriers, Tetracycline

Groundwater is a major source of water in both arid and semi-arid areas[1]. It is an important source of residential, industrial, and agricultural sectors[2,3]. One of the most essential drivers of the nation's sustainable progress is confirming safe and renewable sources of groundwater for the sake of domestic purposes. Nevertheless, the

[1]Department of Environmental Engineering, College of Engineering, University of Baghdad, Baghdad 10001, Iraq. [2]Environmental Research and Studies Center, University of Babylon, Al-Hillah, Iraq. [3]College of Engineering, University of Warith Al-Anbiyaa, Kerbala, Iraq. [4]Department of Civil Engineering, College of Engineering, University of Kerbala, Kerbala 56001, Iraq. [5]Civil and Environmental Engineering, College of Engineering, University of Sharjah, Sharjah, United Arab Emirates. [6]Qatar Environment & Energy Research Institute, Al Rayyan, Qatar. [7]School of Civil Engineering and Built Environment, Liverpool John Moores University, Liverpool, UK. [8]Department of Civil Engineering, Galgotias College of Engineering, Knowledge Park 11, Greater Noida 201310, India. [9]Sustainability Solutions Research Lab, Faculty of Engineering, University of Pannonia, Egyetem Str. 10, Veszprém H, Veszprém 8200, Hungary. ✉email: ayadabedalhamzafaisal@yahoo.com; k.s.hashim@ljmu.ac.uk; osamah.al-sareji@phd.uni-pannon.hu

groundwater quality is often threatened by urbanization, industrial activities, agricultural practices, and climate changes. Toxic metals, hydrocarbons, trace organic compounds, pesticides, and other developing contaminants all pose risks to the health of humans, ecological services, and even long-term socioeconomic developments[4]. In reality, the quality of groundwater is a major environmental concern around the world, and it necessitates the continuous monitoring of a wide range of physicochemical parameters, including cations and anions[5].

Emerging contaminants such as pharmaceuticals and personal care products are making their way into surface water and, to a lesser extent, into groundwater[6]. A wide range of pharmaceutically active compounds (PhACs), including antibiotics, are usually produced and employed on a huge basis around the world. Because pharmaceuticals are often detected in aquatic environments, it is important to evaluate both their harmful impacts on the environment and humans. Antibiotics are among the medications with a high potential for harm to the environment[7–10].

Tetracycline antibiotics (TC) have been traditionally used for treating bacterial infections in humans and animals due to their wide-spectrum bacterial action and low cost. A major characteristic of Tetracycline (TC) is its somewhat high solubility in both methanol and ethanol; however, it has reduced solubility in organic solvents, including ethyl acetate and acetone. About 80% of ingested TC has been discharged into environments from human, and animal feces, and incompletely degraded products[11,12]. Because of its widespread exploitation and its high adsorption capacity, TC is often discovered in both surface and groundwater. On the contrary, wastewater treatment facilities are not capable of removing such micro-pollutants from domestic sewage, which results in its release into the environment[11]. Antibiotic concentrations in the aquatic environment have been removed using a variety of approaches, including bio-treatment and membrane technology, coagulation-flocculation, advanced oxidation processes, wetlands and adsorption[13–16]. Adsorption is considered an effective method, and it has proven to be more efficient than several other wastewater treatment methods[17].

Many adsorbents have been employed for the sake of removing TC from the aqueous environment, such as carbon nanotubes[18], biochar[19], clay-biochar[20], raw bentonite[21], Co_3O_4/Fe_3O_4 nanoparticles, GO/MNPs-$SrTiO_3$[22] and Graphene Sand Hybrid (GSH)[23]. Diverse nanoparticles are capable of purifying wastewater via several techniques including the adsorption of different colours, heavy metals, pharmaceuticals, and other compounds. Nanomaterials are manufactured in various forms and included in a range of composite materials to offer the treatment that is required[24–26]. Brownmillerites are also studied for their magnetic and electric properties due to the possible applications of their ferroelectricity, piezoelectricity, and pyroelectricity. The use of natural resources as chemical compounds for the preparation of nanomaterials was investigated[27].

Pump and treat (P&T), groundwater aeration gas, phase extraction, bioremediation, and in-situ chemical oxidation are examples of traditional technologies that are useful in groundwater pollution remediation[28]. "Pump and treat" (P&T) is a method in which the contaminated groundwater is pumped from the subsurface and then treated before being discharged or reinjected into the aquifer. Despite its adaptability, groundwater rehabilitation generally takes a long time and is unsustainable due to limits imposed by the hydrogeological context and pollutant properties[29]. One of the major techniques being developed as alternatives to the pump-and-treat approach for treating contaminated groundwater is permeable reactive barriers (PRBs)[30].

The PRB method, in conclusion, delivers economic rewards encouraging waste material reuse, thus it introduces a big contribution to environmental sustainability. As a result, it has the potential to be a very practical application in every way[31]. PRBs have been identified as the most appropriate remediation technology that can be utilized to remove pollutants such as heavy metals, chlorinated solvents, carbonates, and aromatic hydrocarbons. The reactive media used to remove pollutants is the most important criterion for a successful PRB[32]. In comparison to traditional technologies, PRB is an important in-situ remediation technique for the polluted groundwater that has been used for several decades. Low cost is needed for operating this technology, which also can't require external power and ground space[33].

PRB is a revolutionary groundwater cleanup technology that is employed all over the world. To facilitate waste disposal, this method combines adsorption, chemical precipitation, and degradation processes to induce physical, chemical, or biological reactions between contaminants and reactive compounds included in barriers[34]. Because of the cheap operational cost, media longevity, and hydraulic performance, the in-situ application of PRB has sparked a lot of attention[35,36]. The longevity of the permeable reactive barrier can rise significantly with thicker beds for low values of inlet concentration and water flow rate, according to research on the barrier's capacity to regulate pollutant migration[37].

Two configurations of PRB have been developed; the first and most common one is continuous PRB and the other is funnel-and-gate. The funnel-and-gate system is constructed of a certain permeable gate (acting as a reactive zone) positioned between a couple of impermeable walls, which drive the polluted plume in the direction of the reactive zone, whereas the design of a continuous PRB is constructed of a single reactive zone spotted across the contamination plume. The decision between the two designs is based on the site's hydrogeological parameters as well as the cost of reactive materials. The funnel-and-gate configuration is preferred when using a high-cost reactive material because the reactive zone requires less material. To maintain utilization and aid in consideration of the consequences for future groundwater supply, it is essential to construct a model for predicting both the short- and long-term operation[38]. To provide a natural gradient for plume flow toward the reactive barrier, these systems are passively operated. In order to optimize groundwater pollution plume capture, funnel gate PRB may provide one or more sizable treatment regions due to certain unique contamination features. The funnel-gate PRB has a small reacting zone and is less difficult to remove and replace when the reactive PRB is clogged with sediments and fine soil particles. Furthermore, several funnel-gate PRB systems can be installed continuously in parallel or in series, depending on the site requirements[39].

On the basis of a thorough comprehension of the observed dynamic behaviour, traditional methodologies like numerical and conceptual models of groundwater have typically been used to forecast the changing hydrogeological state and processes. To define the models of forecast accuracy and reliability, adequate and

appropriate data must be used for the hydrological system's calibration and validation[40]. The numerical or conceptual models are applied for modelling hydrological so as to understand the particular system characterizing, physical processes or for developing predictive tools to estimate appropriate solutions for distributing water, landscape management, surface water-groundwater interaction, or the effects of the new withdrawals of groundwater[41].

Optimization and modelling have become important for the management of contemporary environments. The rising interest in balanced developments triggered different institutions dealing with environmental quality to implement creative solutions for the minimization of energy and working costs. Numerical and statistical methods are most commonly applicable for environmental research and for the comparison of empirical data[42]. Analytical models are applicable for solving simple and idealized contamination transport problems, while numerical models deal with real-world contamination transport simulations[43]. Application of ANN is achieved in many fields, such as water quality modelling[44], management of water quality[45], and nitrate concentration in groundwater[46].

The model representing an ANN can be considered as a driven data model for the simulation of the actions corresponding to biological neural networks in the brain of the human being. An ANN contains a number of variable elements, known as neurons, which can be linked through connections. An ANN is generally constructed of three separated layers: the input layer, the hidden layer, and finally, the output layer. Each layer contains neurons having similar properties[47–49]. The parallel distributed processor driving ANNs manages information from input to output via a certain network of several interconnected nodes. The estimated data in both input and output layers representing the network response as a result of the existing database are known as input patterns, where the hidden or intermediate layer plays a significant role in both representing and estimating complex associations between those patterns[50]. The ability of the ANN model to only learn the correlations between variables; whether linear or non-linear, through a set of instances is its most crucial feature[51].

ANNs have a variety of uses in the study of groundwater quality. In a previous study, an ANN model was created to determine the extent of a polluted zone in an aquifer following an unplanned spill[52]. The application of ANNs has been increased in various fields of science and engineering. Many problems have been successfully solved in groundwater studies using ANNs[53,54]. The ANN models as "black box" models with specific properties are significantly suited to the modelling of the dynamic nonlinear system[55]. The neural network has been adjusted for solving a certain given problem through the process of learning, exploiting typical inducement and response with the proper reaction, therefore, this differs from the classical modelling method, where it is important to define a certain algorithm and create an appropriate program[56]. Two reported ANN limitations included; (i) The size of the network is suitable for a low-dimensional input pattern, such as multispectral data. The number of input neurons increases with hyperspectral data, and an unfeasible number of weights will be assigned to each input by each neuron, and (ii) An ANN is able to process one-dimensional input. This solely refers to spectral information for hyperspectral data. The image pixel data must be transformed into a 1D vector in order to be used as the input for picture or patch recognition and labeling. There are a lot of input neurons in this instance. Another disadvantage is that the classification is based solely on the scant spatial context information contained in the patch or image[57].

The main objectives of the current study are (i) manufacturing of novel reactive material named Brownmillerite ($Ca_2Fe_2O_5$)-Na alginate beads, (ii) finding the ability of such beads in the removal of TC from the contaminated water by batch and continuous operational modes, and (iii) modelling experimental data from continuous tests using ANN approach to predict the value of normalized concentration as function of time-based on the continuous and funnel-gate configurations of PRB.

Experimental work

Chemicals and reagents

In this study, high-purity chemicals were used, which included ferric chloride anhydrous ($FeCl_3$), hydrochloric acid (HCl), sodium hydroxide (NaOH) pellets, calcium chloride ($CaCl_2$) and sodium alginate (with molecular weight 2.5×10^5 and supplied from Sigma Aldrich).

Materials and contaminant

Tetracycline (TC) ($C_{22}H_{24}N_2O_8$) was the intended contaminant. It was supplied from the Samarra drugs factory - Iraq. Chicken bone wastes were used as a calcium source to synthesize Brownmillerite ($Ca_2Fe_2O_5$)-Na alginate beads. The wastes were collected from local restaurants and household wastes. The sandy soil was used to be an aquifer in the tank tests, and the characteristics of (0.6-1) mmm particle size, porosity of 0.48, and specific gravity of (1.36) were provided by the market. The present study used cement kiln dust (CKD) as an impermeable wall in funnel and gate PRB configuration. The CKD was collected from the Al-Kufa Cement Factory - Iraq.

Preparing of Brownmillerite-Na alginate

Brownmillerite ($Ca_2Fe_2O_5$)-Na alginate was prepared as a sorbent for TC elimination from water. Nanoparticles of Brownmillerite can be obtained using the precipitation method[58]. For the preparation of nanoparticles, 250 ml of calcium ions solution (extracted from chicken bone waste) was mixed with 250 mL of iron ions solution (resulting from dissolution of $FeCl_3$), molar ratio of (Ca/Fe = 1). Mixing the two solutions is necessary, adjusting the pH to 10 by NaOH (1 M), and stirring until heavy brownish precipitates are yielded. The precipitates must be separated using Whatman filter paper No.1 and then dried at 85 °C for 12 h. Drying the resulting materials, they must then be washed with DW (2–3) times to remove impurities. Thereafter, the materials were annealed at 200 °C for 8 h and grounded manually to produce ($Ca_2Fe_2O_5$) nanoparticles powder. For manufacturing of $Ca_2Fe_2O_5$-Na alginate, 2 g of Na-alginate can dissolve in 100mL of DW and the resulting solution must be stirred using a magnetic stirrer for 24 h at room temperature. The prepared $Ca_2Fe_2O_5$ nanoparticles (5 g) were

combined with Na-alginate solution. For beads polymerization and formation of $Ca_2Fe_2O_5$-Na alginate beads, the slurry was brought into a solution of ($CaCl_2$ with 0.1 M) using a 10 mL syringe. The beads were drying at 105 °C. Figure 1 illustrates the synthesis procedure for preparing Brownmillerite-Na alginate beads.

Batch experiments

The equilibrium of TC adsorption onto Brownmillerite ($Ca_2Fe_2O_5$)-Na alginate beads was examined through a series of batch experiments. The experiments are designed to detect the suitable values of operating parameters including contact time, initial concentration (C_o), initial pH, agitation speed and mass of adsorbent that is necessary for removing the most molecules of TC for selected C_o. Several conical flasks (100mL) have been filled with 50mL simulated from contaminated water (V). This water was mixed with different masses of prepared adsorbent (m). The flasks must agitate for 3 h at 200 rpm. At ending of each test, filter paper should be used to separate the adsorbent from the water, and the concentration of TC at equilibrium (C_e) can be measured using a UV spectrophotometer. Equation 1 can be applied to estimate the TC quantity retained on the adsorbent at the equilibrium (q_e) based on the values of C_o and C_e[59]. The operating conditions of batch tests involved contact time (0.1-3) h, initial of tetracycline (C_o) of (100–250 mg/L), pH (3–12), agitation speed (50–250) rpm and dosage of adsorbent (0.2–1.2) g/50 mL. Each point of sorption measurements that obtained in the batch study is the average value for three readings.

$$q_e = \frac{(C_o - C_e)\,V}{m} \tag{1}$$

Continuous experiments

Column operation mode (one dimension 1D)

The experimental setup employed for the simulation of TC migration that dissolved in water consisted of a Perspex column, a water tank, a valve, a peristaltic pump and tubes. The column dimensions of 2.5 cm as inner diameter, 35 cm as height, and 3 mm as wall thickness as it is obvious in Fig. 2. For reflecting the real conditions in the packed column, TC migration was assumed to be in a single dimension within the column bed for the sake of achieving uniformly moving water. The column was filled with 30 cm of beads to evaluate their efficacy in reducing tetracycline concentration. The distilled water was pumped upward from the bed bottom to avoid trapped air. The TC-contaminated water was added after that to the bed at 5, 10, and 15mL/min until reaching the stage of saturation. The flow parameters of the groundwater have been determined to ensure that such a flow is laminar. The ports P1, P2, and P3 of the columns are placed at 10, 20, and 30 cm, respectively, from the entrance of the column. For measuring the TC concentrations, the samples of water were brought out of the ports at certainly precise intervals. The initial concentrations of TC in the influent were 100, 150, 200, and 250 mg/L.

Tank operation mode (two-dimensional 2D)

In a two-dimensional tank, the simulated TC transport was carried out. This bench-scale model aquifer is contained inside a rectangular Perspex glass tank that measures (100 cm × 40 cm × 10 cm) with 6 mm thick glass sheets. The tank's entire outside was transparent to enable visual inspections. The rectangular tank was divided into three parts: the middle compartment and the influent and effluent chambers. Partitions were made by two perforated vertical boards covered with a filtration screen. The partitions were considered as lateral boundaries of the middle compartment which had dimensions of 80 × 40 × 10 cm (Fig. 3). The purpose of the influent and effluent chambers was to regulate the water table's position inside the model aquifer that was deposited in the middle compartment as well as the moisture of the aquifer mass. The dimensions of each chamber are 10 cm long, 40 cm wide, and 10 cm deep. Funnel

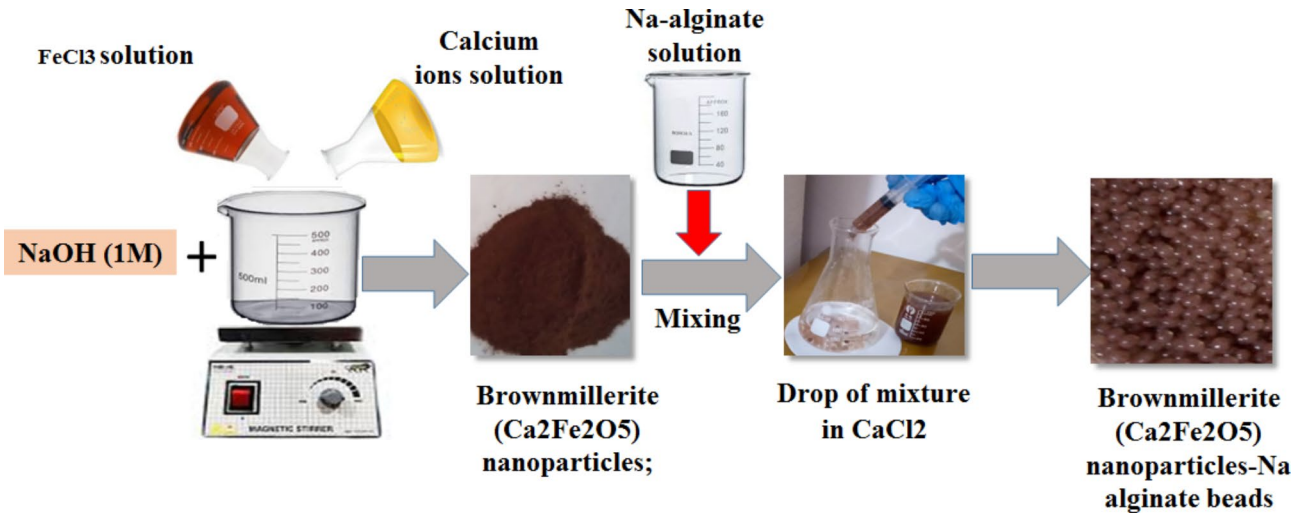

Fig. 1. Flowchart for preparing Brownmillerite ($Ca_2Fe_2O_5$)-Na alginate beads.

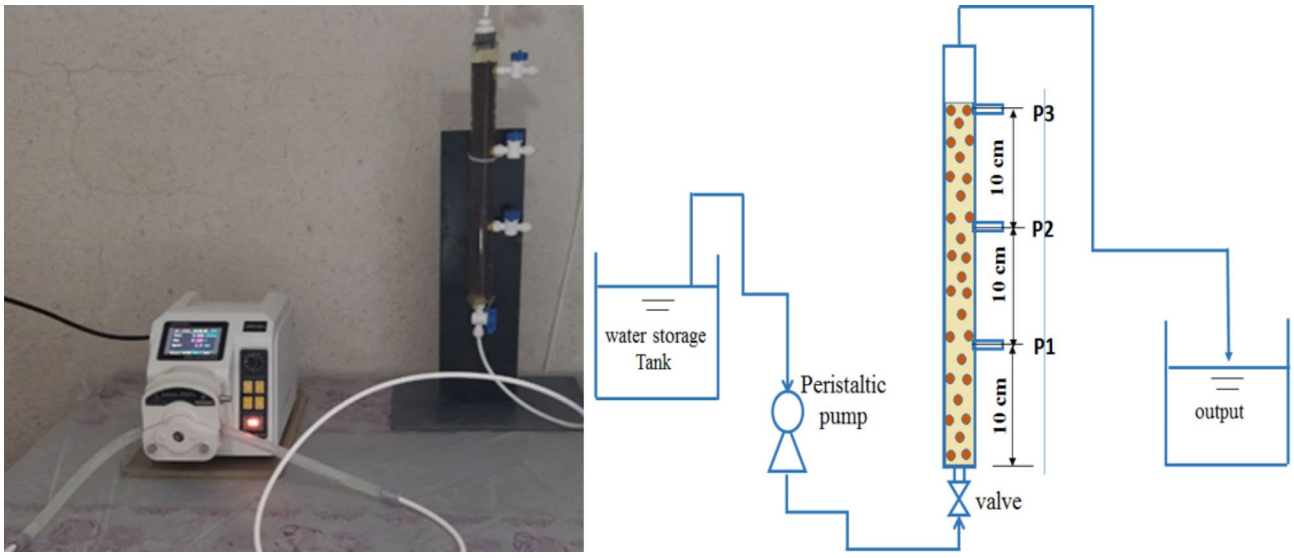

Fig. 2. Column setup used for monitoring of TC front in the one-dimensional operational mode.

Fig. 3. Tank setup used for monitoring of TC front in the two-dimensional operational mode of funnel and gate configuration.

and gate configuration was employed in two dimensions experiments. The dimensions of the reactive gate are a length of 20 cm, a width of 10 cm and a depth of 5 cm. Two angles of the funnel were adopted in this study (45° and 30°). The middle compartment consists of measuring from the left-hand side: (i) sand with the dimension of (60 cm × 40 cm × 5 cm), (ii) reactive gate (20 cm × 10 cm × 5 cm) in addition to funnel, and (iii) sand with dimension of (40 cm ×10 cm × 5 cm). The sampling ports P1, P2, and P3 are set up at distances of 60, 65, and 70 cm, respectively (Fig. 4). Stainless syringes were used to collect samples at scheduled intervals. The source of the contaminated solution was introduced to the middle compartment through the influent chamber (10 cm ×10 cm×10 cm), which represented a continuing discharge of contamination at rates of 500 and 1000 mL/min.

Results and discussion

Operating parameters in batch experiments

Various operating parameters were considered in batch tests including contact time, initial concentration of TC, agitation speed, pH and mass of sorbent. The contact time is the crucial step in the determination of the TC distributed between the solid and liquid phases in the batch experiments that can satisfy the equilibrium condition. Figure 5(a) illustrated the variation of sorbed quantity (q_e) as a function of contact time up to 3 h at C_o of 100 mg/L, pH 7, sorbent dosage of 0.5 g/50 mL and speed of 200 rpm. The TC adsorption capacity can increase at a high rate at the beginning of the test, and this rate may reduce after 1.5 h because of the decrease in the vacant sites[60,61]. The outcomes show that the TC adsorption capacity was 5.151 mg/g at 1.5 h; however, there is no notable increase in the sorbed quantity beyond this time till 3 h.

Figure 5(b) illustrates that the sorbed quantity of TC is affected significantly by the initial concentration of TC (C_o). The sorbed quantitates were substantially declined, from 5.151 to 3.887 mg/g when C_o vary from 100 to 250 mg/L respectively at 1.5 h, pH 7, sorbent dose of 0.5 g/50 mL and agitation speed of 200 rpm. For lower concentrations, it is expected that all TC molecules will interact with the available binding sites, which

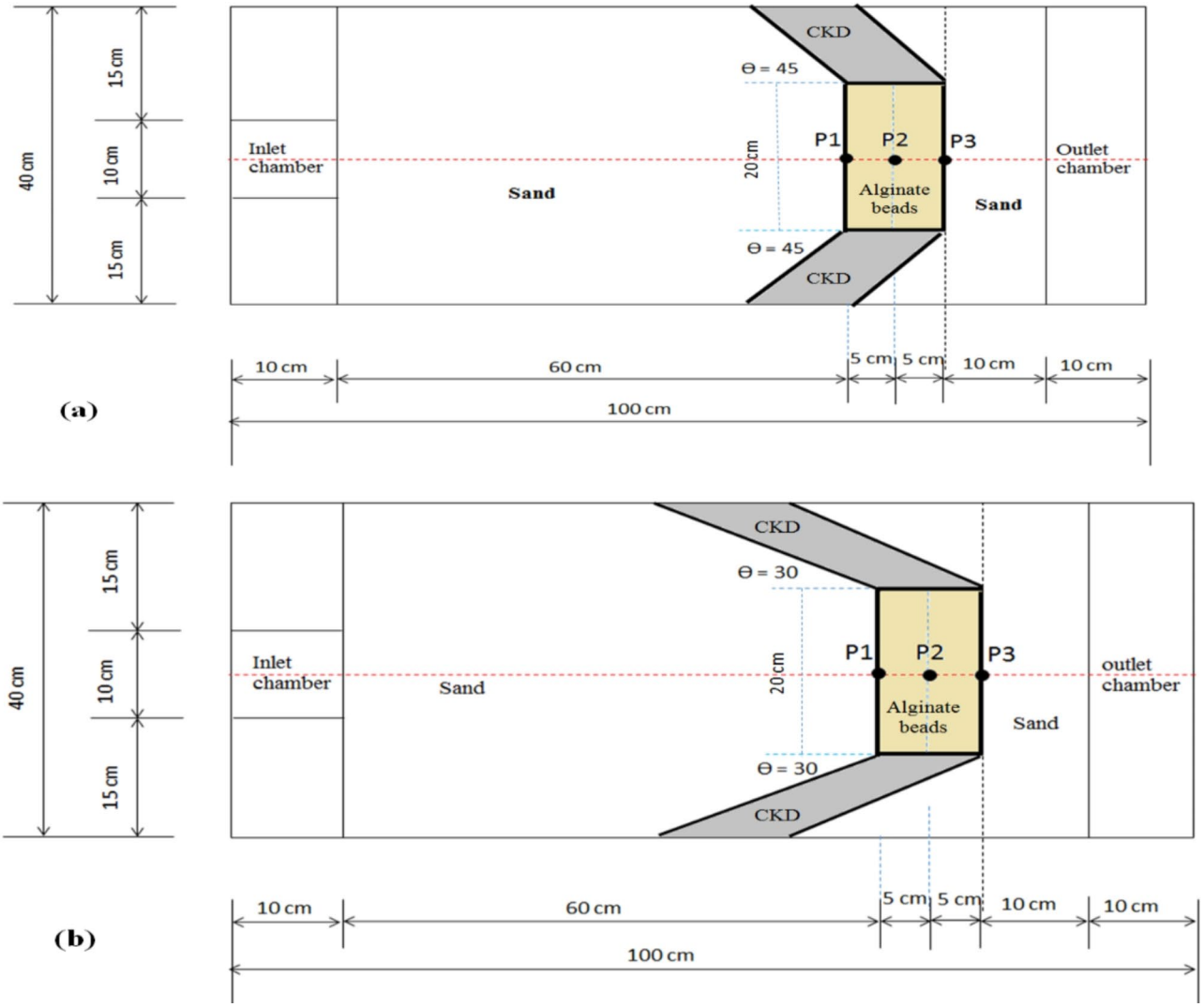

Fig. 4. Schematic diagram of funnel and gate applied in the PRB configuration.

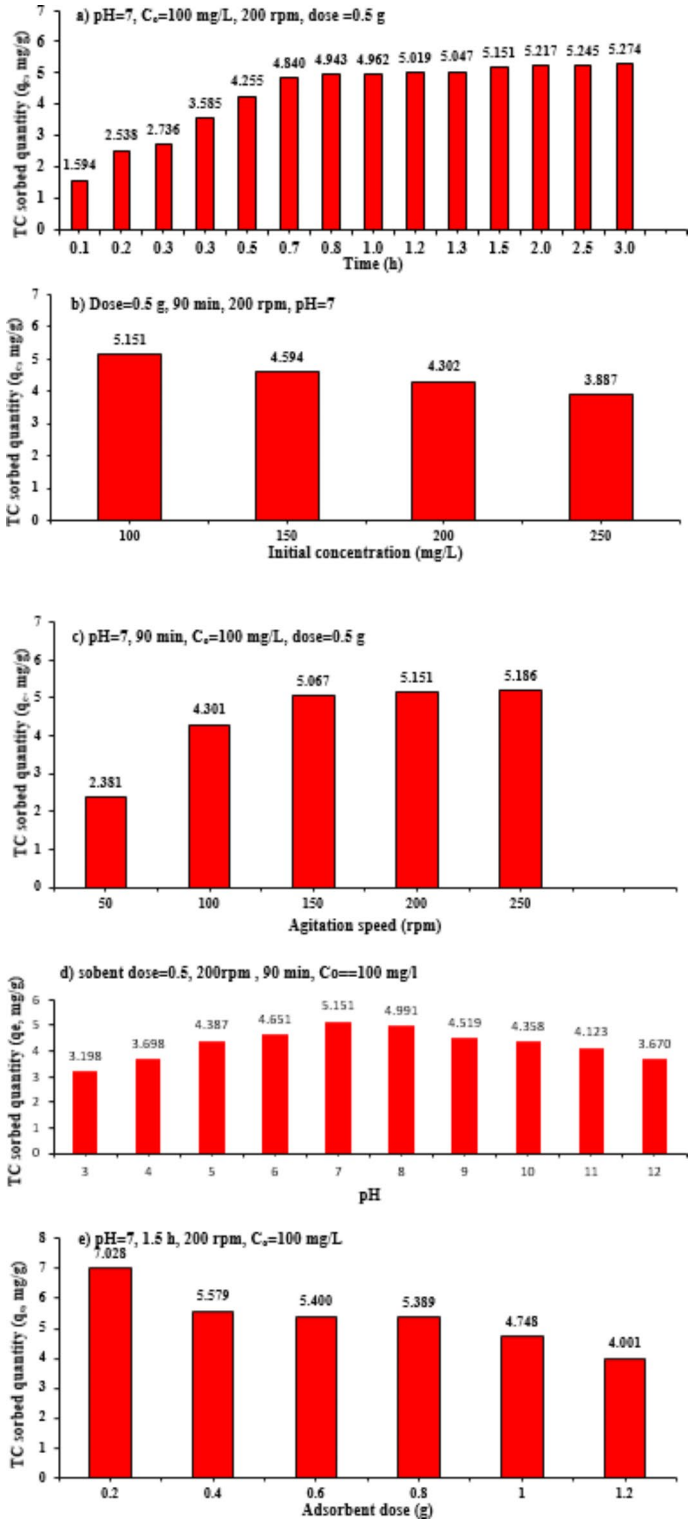

Fig. 5. Impact of operating parameters in batch tests; (**a**) contact time, (**b**) concentration of TC, (**c**) speed, (**d**) pH (**e**) adsorbent dose.

will certainly result in a noticeable increment in the adsorbed quantity of TC; however, a large number of TC molecules resulting from an increase in concentration with particular grams of sorbent may lead to decrease in the sorbed quantity[62,63].

Figure 5(c) shows the impact of agitation speed on the adsorbed quantity of TC. It is obvious that when the agitation speed is increased, the adsorbed quantity of TC is increased. In fact, when the agitation speed is high, it accelerates the diffusion of contaminants within the beads, which promotes a suitable interaction between the

contaminant and binding sites. Additionally, it was determined from the data that an agitation speed of 200 rpm was adequate to achieve maximum TC uptake and that there was no discernible difference in the removal after this speed.

The pH of the solution is considered a significant factor in the TC sorption from aqueous solution. It affects the adsorbent surface charge, functional groups dissociation and ionization degree. The adsorbed quantities of TC are plotted versus different values of initial pH, ranged (3–12), as shown in Fig. 5(d). The adsorbed capacity of TC was low (3.198 mg/g) at pH 3.0 because the H^+ ions may compete with TC antibiotic molecules. The sorption capacity may be revealed to improve obviously as pH is closer to neutral, reaching values of 5.151 mg/g at pH 7. The hydration of antibiotics and ionization may decrease when the condition is neutral, which may accelerate sorption by promoting hydrogen bonding and π-π - stacking effect. The beads and TC are expected to be most attracted to one another when the pH is neutral, which is congruent with TC's maximum uptake at neutral pH. The adsorbent will yield electrostatic repulsion with the TC when pH is more than 7, which eliminates the adsorption performance. Consequently, electrostatic repulsion is the primary form of electrostatic interaction between TC and beads. The adsorbed quantity decreases because of changes in the pH solution towards more than 7. This is due to the generation of the OH ions, which leads to attenuation in the bonding of hydrogen.

The effect of beads amount on the TC adsorption was investigated in the range from 0.2 to 1.2 g per 50mL of the contaminated solution in order to obtain the optimum dose for C_o of 100 mg/L, time 1.5 h, and pH 7 at 200 rpm. Figure 5(e) illustrates the variation of (q_e) for TC as a function of adsorbent mass. It is obvious here that the TC removal capacity may decrease with a greater mass of beads for the same TC initial concentration. This can be justified by the condition that while the dosage of the alginate beads increased, the number of effective areas and vacant sites built up. Consequently, a smaller adsorbent mass is capable of adsorbing more molecules of tetracycline[64]. The adsorbed quantity ranged from 7.028 mg/g at 0.2 g to 4 mg/g with 1.2 g of the beads. Table 1 compares prepared sorbent and others in the literature for removing TC.

Characterization analysis

The X-ray diffractometer (XRD) analysis is exploited to demonstrate obtaining the patterns of diffraction for adsorbent created from oxides of both iron and calcium applied with 2θ values ranging from 10° to 80°. Such an analysis validated ($Ca_2Fe_2O_5$) formation. This is due to the numerous diffracting reflections generated at certain intensities of 27.575^0, 29.475^0, 31.775^0, 45.53^0, and 56.73°. It is important to note that the active sites in beads, which are able to remove TC out of an aqueous solution, have been depicted through such reflections. The FT-IR spectra corresponding to the beads produced before and after the TC sorption are accomplished to recognize primary functional groups and enhance antibiotic adsorption, as shown in Fig. 6. The test explains that the amides and the (-OH) groups experience stretching vibrations that lead to the formation of bands of high-intensity absorption. The peaks corresponding to alginate beads have demonstrated a strong and wide absorption band at frequencies of (3550–3200 cm^{-1}), which was stimulated via the stretching vibration corresponding to hydrogen bonds and stretching mode created by OH groups. Peaks at 3431.71, 2924.52, and 2847.38 cm^{-1} are corresponding to the stretching vibrations of OH and C—H, respectively. Peaks at 1628.51 and 1418.39 cm^{-1} are directly related to the stretching vibrations of O–H and stretching vibrations corresponding to -COO-(symmetric), respectively. Weak bands occurring at 1033 cm^{-1} are related to the C-O stretching of both COO- and the C-O-H groups[71]. The stretching vibrations of Ca-O and Fe-O (including ferrite skeleton) bonds correspond to the bands of absorption at 309.228, 442, and 564.077 cm^{-1}[72]. SEM graphs can be used to describe the morphological characteristics of produced beads after and before contact with tetracycline, as illustrated in Fig. 7a,b. The mean rod particle is shown in Fig. 7a, which shows that the prepared sorbent's porous surfaces have nonhomogeneous morphology at 200 nm magnification scales, this surface might be incredibly compact and disordered. The beads' surface appears to be macro-porous, allowing oxyanions to be absorbed. There are noticeable morphological changes in the beads following the removal of TC when compared to the sorbent before the sorption process.

Potential adsorption mechanism

Generally, many interactions improve TC adsorption in aqueous solution, including electrostatic interaction, cation- π interaction, hydrogen bonding, and intra-particle diffusion. However, the pH solution and TC concentration, characterization analysis of adsorbent have significant impact on the overall mechanisms interaction of adsorption process. Prepared beads contain various functional groups which may have acidic or alkaline properties. Based on the surface chemistry and sorbent structure, the most likely processes for TC

Adsorbents	q_e (mg/g)	Contact time (h)	C_o (mg/L)	pH	Ref.
ZnAl-LDH/BGC	41.98	2	25	6	[65]
NCPML	4.65	3	5	4	[66]
Re-generable pumice	3.345	24	40	6	[67]
Fe-doped zeolite	200	24	-	6	[68]
ATMa	12.58	0.5	-	2	[69]
PAM/CA@Cu	356.57	-	100	5	[70]
Brownmillerite (Ca2Fe2O5)–Na alginate beads	7.845	1.5	100	7	This study

Table 1. A comparison of prepared sorbent with other existing adsorbents for tetracycline (TC) removal.

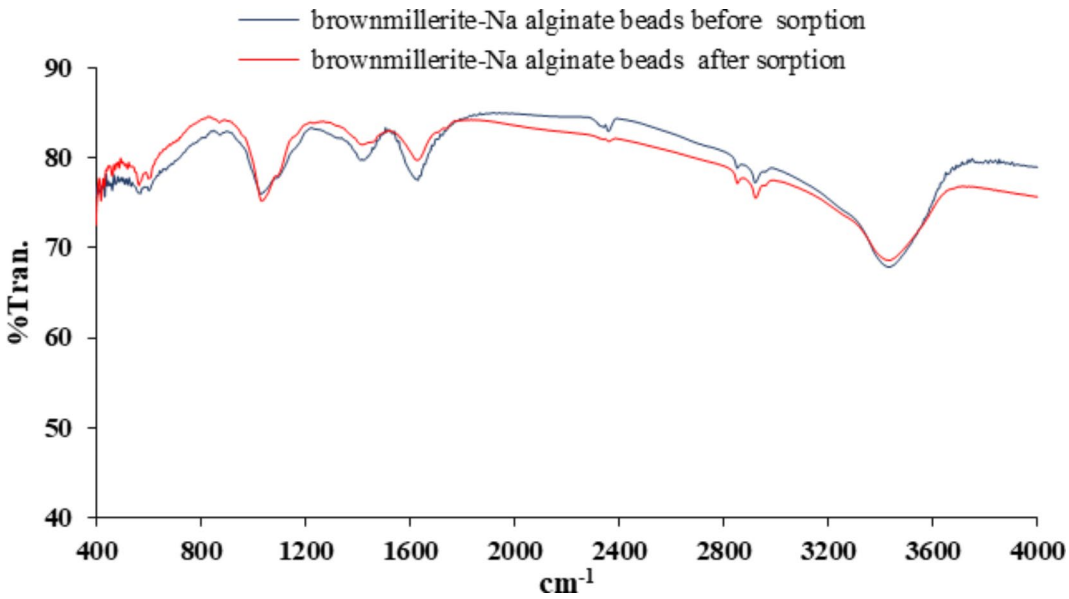

Fig. 6. FT-IR analysis for Brownmillerite-Na alginate beads before and after sorption.

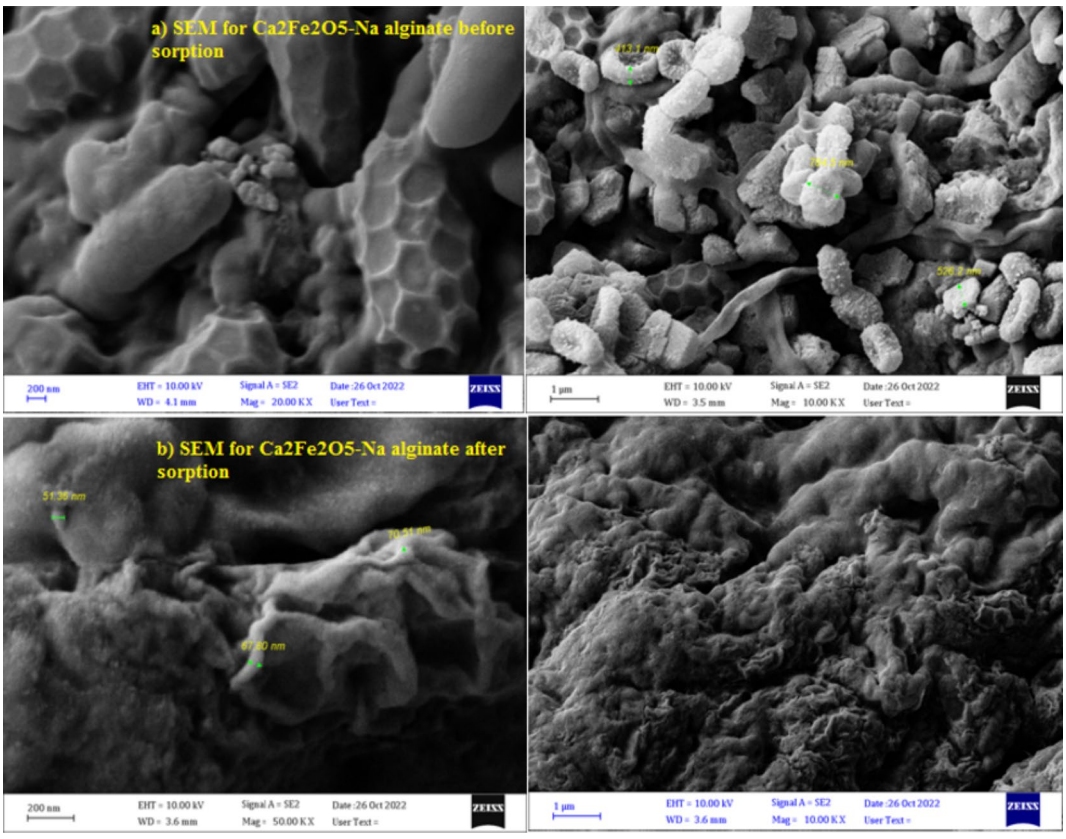

Fig. 7. SEM graphs for Brownmillerite-Na alginate beads before and after sorption.

adsorption onto beads have been identified using FT-IR spectra[73]. The groups calcium (Ca-O) and (Fe-O) in the beads may interact with the functional groups of the positively charged quaternary ammonium and negatively charged phenolic diketone moiety corresponding to TC species[74]. Hydrogen bonding may be removed Tetracycline via surface complexation with hydroxyl groups (-OH) on beads. Surface complexes between Ca on nanoparticles of beads and oxytetracycline with the constitution of the surface complexes between tetracycline and Ca may have occurred. After the TC adsorption process, intensity variation of FT-IR spectra was showed

with decreasing intensity of (C-O) and (Ca-O) on the surface, may be suggested that oxygen in the carbon and calcium groups in calcium iron oxide could be considered as the favorite site for the adsorption of TC. Such interactions include hydrogen bonding or electrostatic attractions between oxygen in calcium iron oxide and amino groups (-NH2) that exist in TC[75].

Developing and optimization of ANN model for continuous tests

A neural network model using the Levenberg-Marquardt backpropagation (LMA) training algorithm was constructed to compare the effectiveness of Tetracycline removal from aqueous solution using the sorption technique with beads in the one and two dimensions (Fig. 8). The neural network's architecture was described, specifying the number of layers, nodes within each layer, and the types of transfer functions employed. The experimental data were classified as training, validation, and test subsets, accounting for 60, 20, and 20% of the data, respectively. This partitioning of the original experimental data facilitated the modelling of the artificial neural network (ANN) and was crucial for comprehending its architecture. The implementation of this approach was carried out using the Matlab application, specifically version 7.10.0.499 (R2010a).

The neural network acquires knowledge of patterns present in the data by adjusting the network weights based on the training data, which constitutes the largest subset. The validation data serves as a final evaluation of the trained network's performance and ability to generalize, while the testing data is employed to evaluate the overall quality of the network. In this study, a linear transfer function (purelin) was employed at the output layer, while a tangent sigmoid transfer function (tansig) was used at the hidden layer. For the one-dimensional system, the feed-forward neural network considered the input variables of initial concentration (mg/L), flow rate (mL/min), time (min), and bed height (cm). In the case of the two-dimensional system, the input variables included initial concentration (mg/L), flow rate (mL/min), duration (min), bed width (cm), and impermeable wall (funnel) angle. The normalized concentration (C/C_o) was chosen as the output variable in the experimental study. The topology of ANN model was optimized using the least mean square error (MSE) for both the training and prediction sets, as shown in Fig. 9. Initially, the model was built with two hidden neurons, but as more neurons were added, the MSE values progressively decreased, leading to improved performance, as indicated in Fig. 9.

The mean square error (MSE) of the 1D network varied between 0.0084 for 2 hidden neurons and a maximum value of 0.0107 for 3 hidden neurons, as presented in Fig. 9(a). Once it reached its minimum value of 7.09E-04 with 30 hidden neurons, the MSE experienced a significant decline. This particular value was determined to be the optimal choice for the specific scenario under investigation. Subsequently, the MSE increased to 0.0012 when the number of neurons reached 35. This rise can be attributed to the characteristics of the input vector and the MSE performance metric employed in the present study. The MSE of the 2D network varied between 0.0204 for 2 hidden neurons and a maximum value of 0.05 for 9 hidden neurons, as presented in Fig. 9(b). Once it reached its minimum value of 0.0029 with 59 hidden neurons. Figure 10 clearly demonstrates a consistent relationship between MSE and the number of hidden neurons for all considered scenarios.

The training process for the 1D and 2D Levenberg-Marquardt algorithms (LMAs) was concluded after 43 and 44 epochs, respectively. This decision was made due to the growing discrepancies observed between the

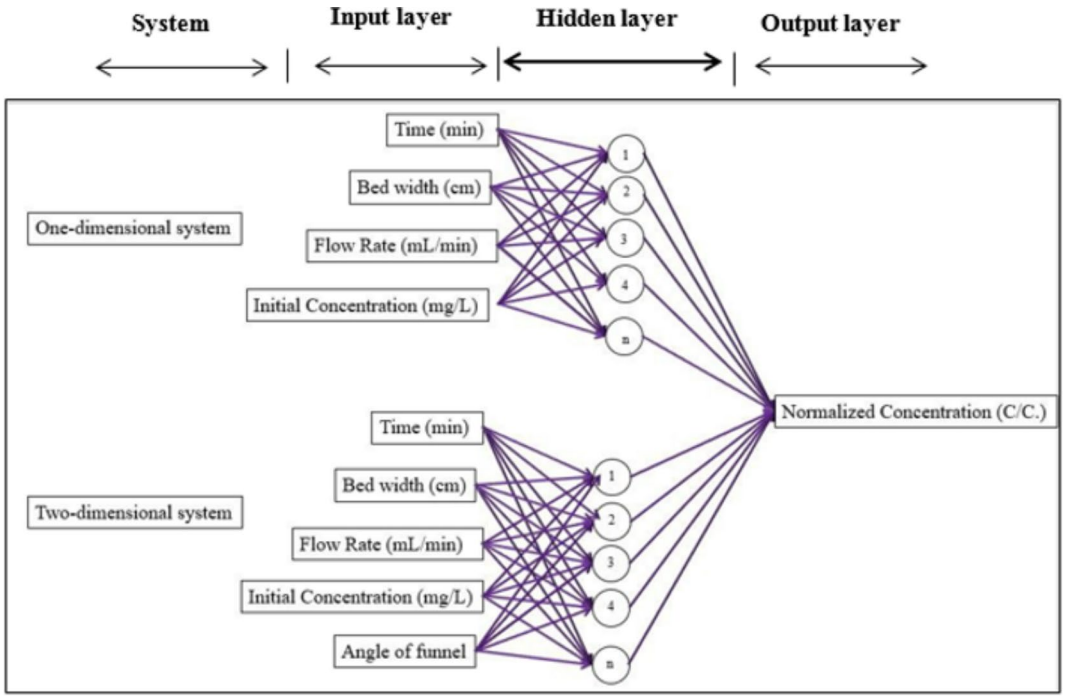

Fig. 8. The optimal architecture of the ANN.

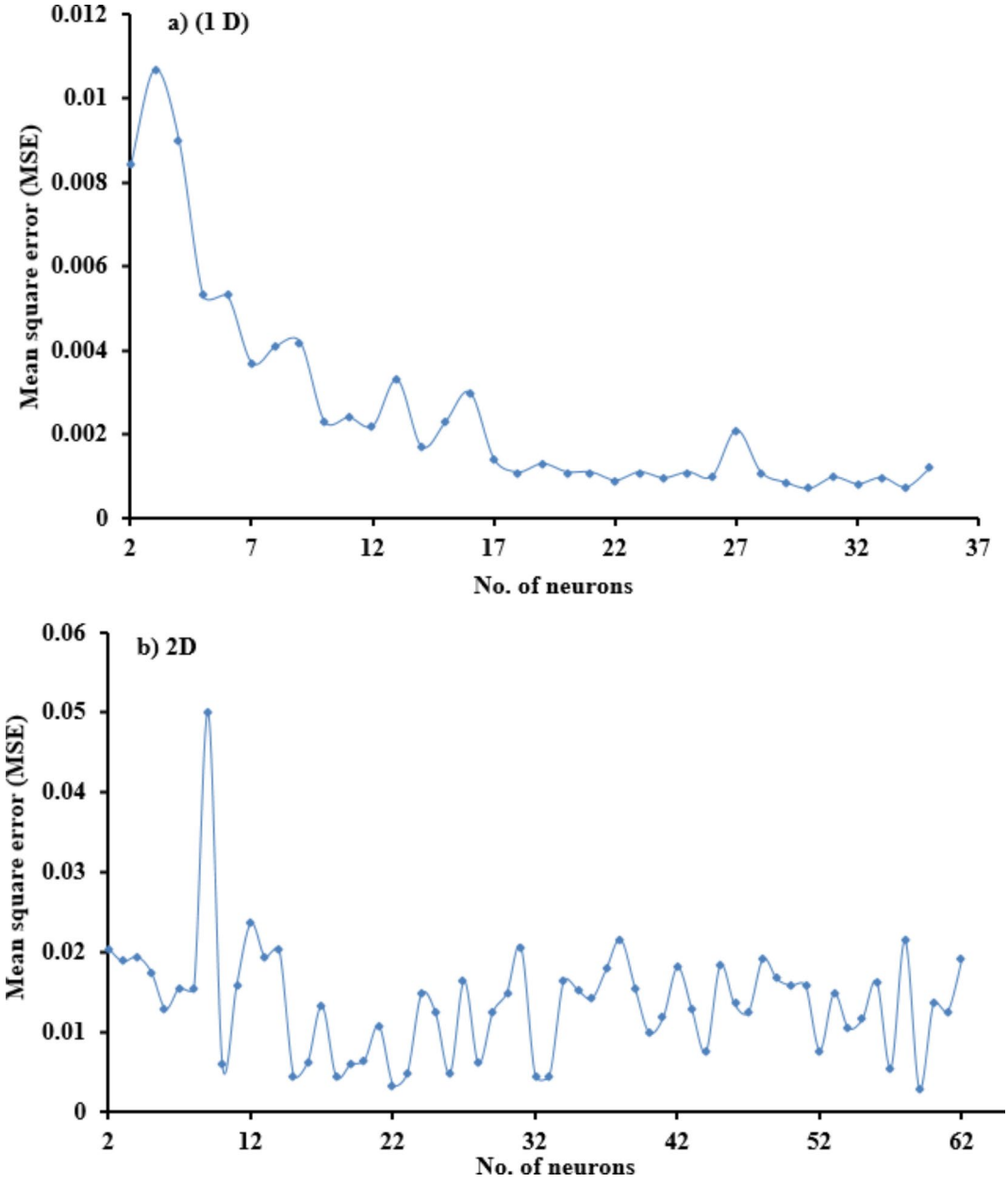

Fig. 9. Dependence between MSE and number of neurons at hidden layer for the LMA.

training error and validation error. The mean square errors for training, validation, and test sets are depicted in Fig. 10. Additionally, Fig. 11 shows cases of the optimal regression achieved through the training, validation, and testing phases using the Levenberg-Marquardt method. Correlation coefficients for training, validation, testing, and the entire dataset are illustrated in Fig. 11.

Breakthrough curves

Column tests (one-dimension system 1D)

The influence of inflow concentration on the spread of breakthrough curves for the adopted TC through the bed at a constant flow rate of 5 mL/min is depicted in Fig. 12. Within the concentration range of 100–250 mg/L, variations in the inflow concentration directly impact the spread of the breakthrough curves. The saturation rate of the bed is subject to changes in the concentration gradient. At lower influent concentrations, the presence of sluggish sorption can make the curve shape less discernible. However, increasing the influent concentration can lead to a steeper slope in the curve, facilitating a quicker saturation of the sorbent. Furthermore, a low concentration gradient results in an extended saturation period as it hinders the contaminant's movement within the pores, mainly due to a reduction in the mass transfer and/or the coefficients of diffusion[61,76]. This can impact TC sorbed amounts within the bed at the point of breakthrough (q_b) and the saturation point (q_s). The values of

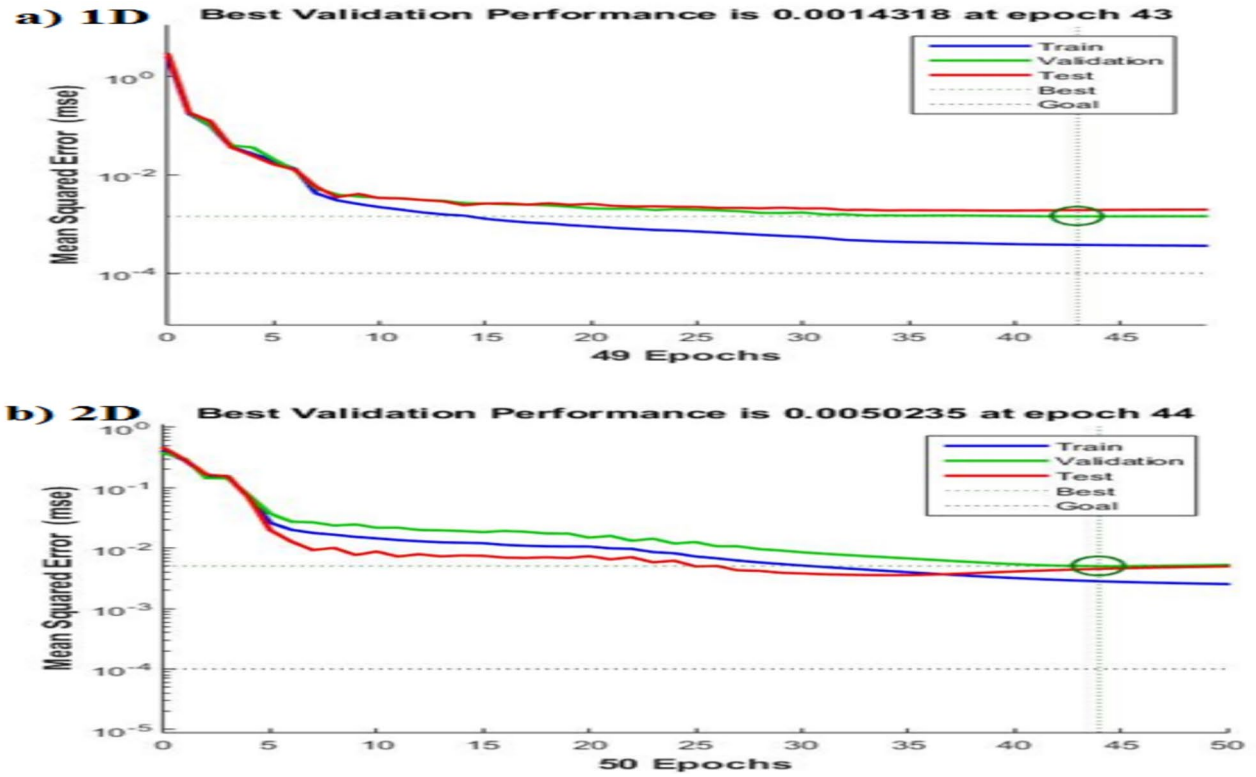

Fig. 10. The mean square errors of training, validation and test for the Levenberg–Marquardt algorithm.

C/C_o, which represent the normalized concentration, reach 5% for breakthrough time (t_b) and 95% for saturation time (t_s). A decrease in the normalized concentration leads to an increase in these times[77].

The sorption of tetracycline onto a bed was investigated using three different flow rates: 5, 10, and 15 mL/min, with a constant influent concentration (C_o) of 100 mg/L (Figs. 12 and 13). These figures illustrate the breakthrough curves for the adsorption of TC at different locations within each packed bed, corresponding to the respective flow rates. It is observed that increasing the flow rate leads to a decrease in the breakthrough time (t_b) and an increase in the curve's steepness. This phenomenon suggests that the time of residence is insufficient and hence the contaminated solution will exit before reaching equilibrium. The presence of a concentration gradient within the layer of mass transfer surrounding the particles facilitates the transfer of mass from the liquid phase to a solid matrix. Increasing the flow velocity can reduce the solute's affinity for the sorbent, resulting in a decrease in sorption efficiency[78]. Figures 12 and 13 illustrated the impact of varying the bed depth (10, 20, and 30 cm) on the sorption process. The results demonstrated that a larger amount of sorbent enhances the sorption capacity under the same operating conditions. As the bed depth increases, the formation of the plume front takes longer, thus potentially extending the breakthrough time. These figures present a comparison between the experimental data and the predictions obtained from the network model for TC concentrations at different time intervals during pollutant transport, considering a specific initial concentration and flow rate. The artificial neural network model exhibited excellent performance with correlation coefficients exceeding 0.98 for the operating variables, demonstrating its accuracy and effectiveness in predicting the experimental outcomes. This chemical could prove valuable in the development of treatment facilities designed to remove tetracycline from wastewater, and it could also be employed as a reactive permeable barrier to remediate contaminated groundwater.

Tank tests (two-dimension system 2D)

A two-dimensional method proves to be an effective and efficient approach for quantifying the distribution of contaminants in both the PRB and aquifer systems. In the current study, where the influence of concentration, flow rate, and the angle of the permeable reactive barrier in both the X and Y directions is considered, the implementation of ANN to simulate this system is deemed appropriate. The anticipated results from this statistical model show the behaviour of the PRB after 0.4 days for flow rates of 500 and 1000 mL/min. Figures 14 and 15 present the X-Y plane of the normalized concentration of TC throughout the laboratory's 2D pack tank in the presence of alginate beads. Both the magnitude and dispersion of the contaminant plume are significantly affected by the applied flow rate (flow velocity). Consequently, the extent of the plume is larger in the longitudinal (X) direction compared to the transverse (Y) direction, and the greatest concentrations are observed in the up-gradient sand bed of PRB. These figures provide a comparison between the experimental data and the predicted results at specific monitoring points during the migration of the TC plume at various time intervals for flow rates of 500 and 1000 mL/min. The concentration levels at ports P1, P2, and P3 placed along with the centerline of the

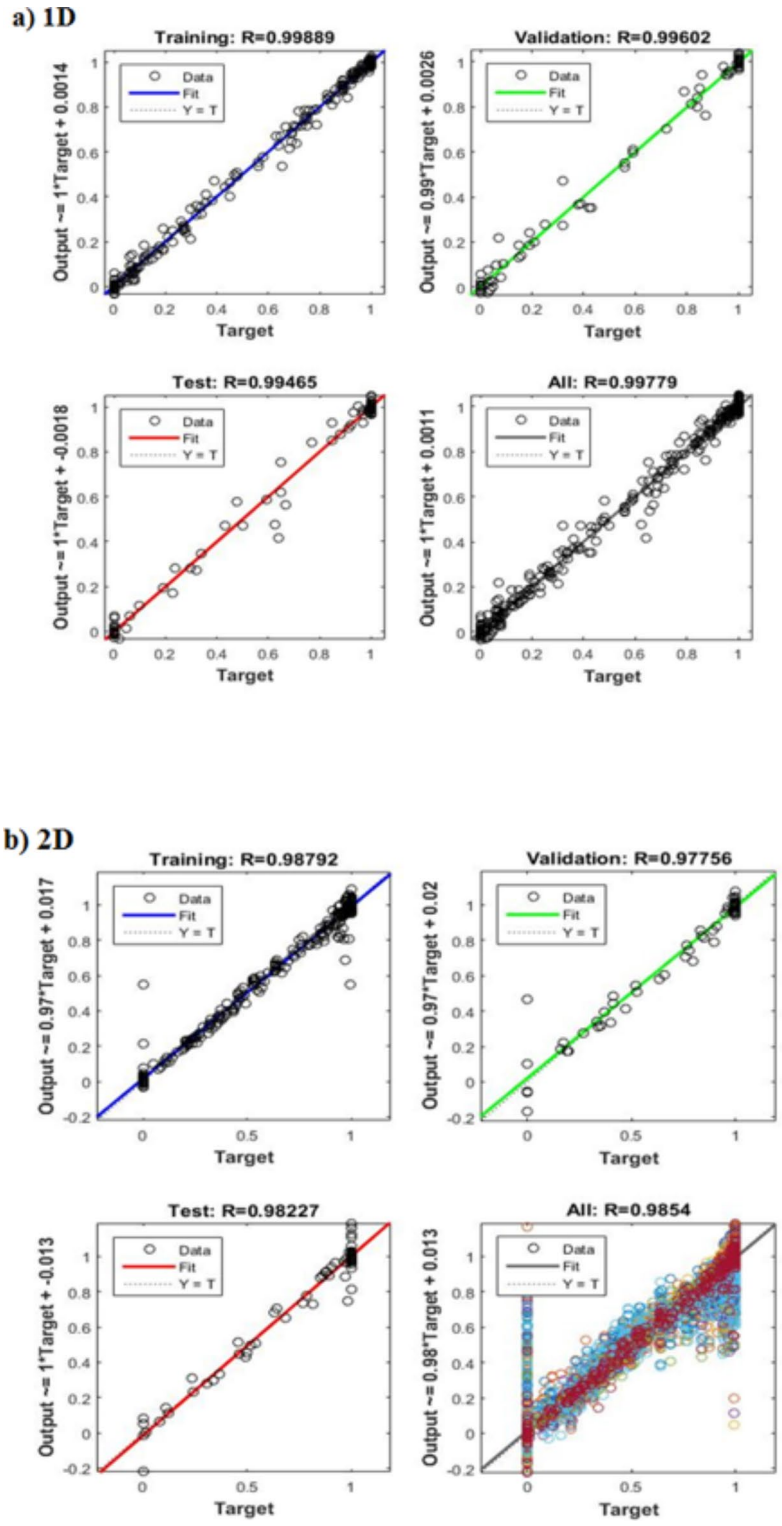

Fig. 11. The testing regression of training, validation and the Levenberg-Marquardt algorithm.

source region (Y = 20 cm) exhibit consistent spatial and temporal concentration profiles. It is evident that the PRB effectively slows down the migration of pollutants in its downward gradient side. However, over time, the barrier's performance is expected to decline due to the reduction in the retardation factor. Conversely, increasing the thickness of the barrier enhances the retardation efficiency of the barrier.

Theoretical studies indicate that the removal efficiencies of the sodium alginate particles are not significantly different from one another. The expected and experimental results demonstrate a reasonable level of agreement. It is common practice to report calibration results by calculating the average discrepancy between the measured

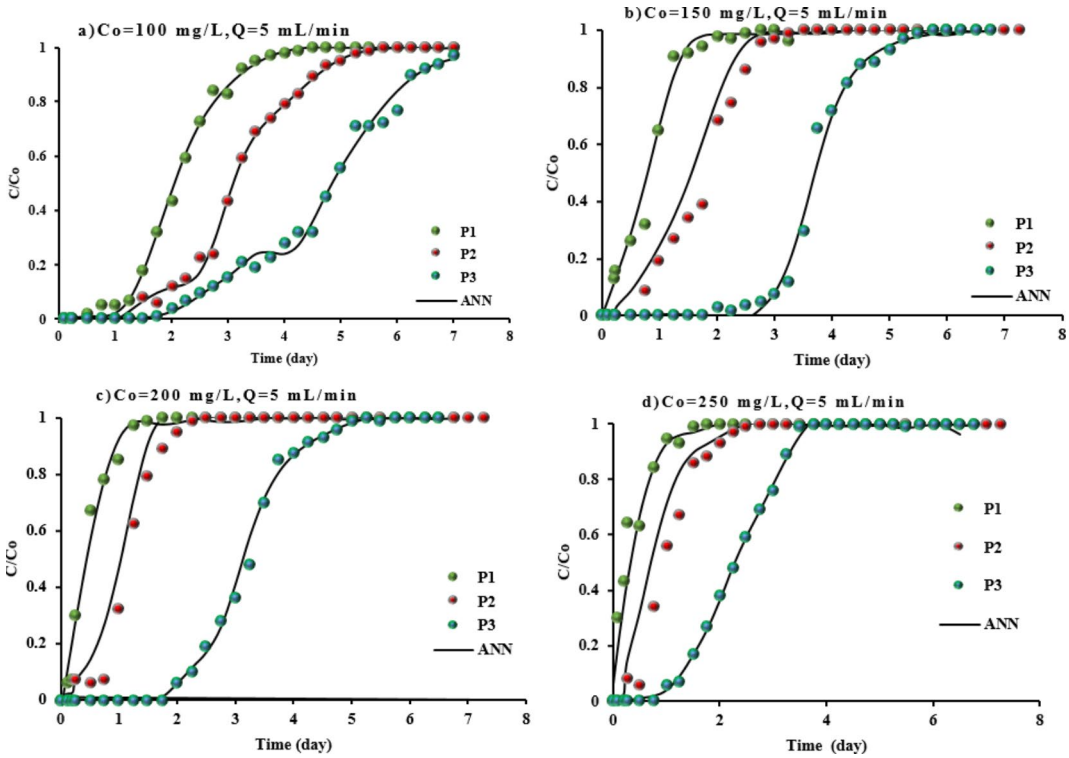

Fig. 12. Comparison between measurements of (1D) system and outcomes of ANN for TC sorption onto adsorbent at different ports for flow rate = 5 mL/min and initial concentration = 100, 150, and 250 mg/L.

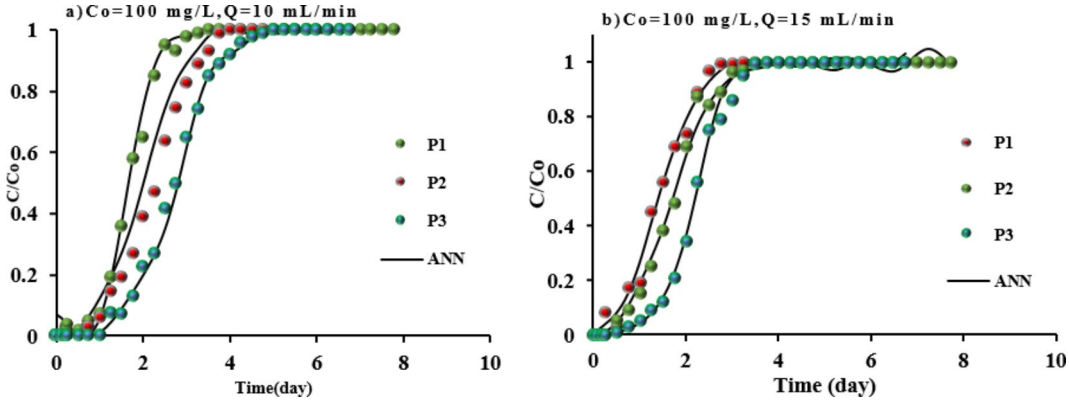

Fig. 13. Comparison between measurements of 1D system and outcomes of ANN for the sorption of TC onto sodium alginate particles at different ports for initial concentration = 100 mg/L, flow rate = 10 and 15 mL/min.

and simulated concentration values. The correlation coefficients, which indicate the average difference between the simulated and actual concentrations, were found to be higher than 0.98. This discrepancy can be attributed to the computational model's omission of salt sorption and its competition with the metal on the surface. Salts such as calcite or carbonate, which can dissolve from groundwater and soil contact, were not taken into account in the present computational model. Figures 14 and 15 display the breakthrough curves illustrating the anticipated and the experimental normalized concentrations increase over time at the ports P1, P2, and P3 placed along with the centerline of the source region (Y = 20 cm) for a certain flow rate of 500mL/min. Such a concentration of the solute exhibits a gradual rise until it reaches a steady-state asymptote. Such curves demonstrate the variation in pollutant concentration between the up-gradient and down-gradient of PRB, highlighting its potential effectiveness in the remediation process. Although, with time, the profiles of concentration exhibit similar patterns as depicted in these figures, there are some discrepancies between the anticipated and experimental results. These disparities can be attributed to several factors; Firstly, the neglect of salt adsorption in addition to their competition for contaminant adsorption over the solid surface of the aquifer could contribute to the observed differences, and Secondly, the rate of contaminant adsorption can be influenced

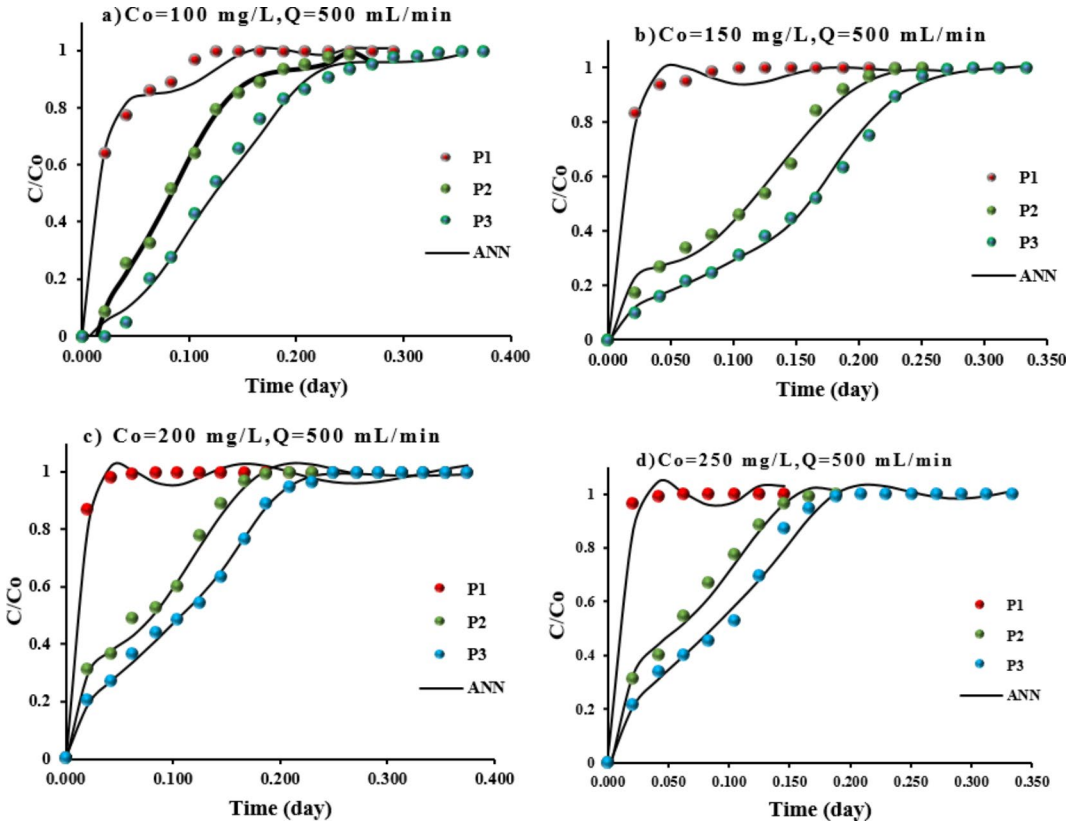

Fig. 14. Comparison between measurements of 2D system and outcomes of ANN for the sorption of TC onto sodium alginate particles at different ports for flow rate = 500 mL/min, initial concentration = 100,150,200 and 250 mg/L and angle of impermeable walls = 45°.

by different environmental factors during water flow through the porous media employed in the study, including pH, contaminant affinity, and other relevant parameters. Considering these factors, it is understandable that there may be variations between the expected and observed outcomes.

Figures 16 and 17 illustrate the distribution of normalized TC concentrations in the two-dimensional packed tank in the presence of the PRB after 0.4 days for flow rates of 500mL/min and 1000 mL/min, respectively. The concentration contours demonstrate that the barrier effectively prevents the contaminated plume from spreading in both up-gradient and down-gradient regions. It is also evident that the applied flow rate plays a significant role in the size and concentrations of the contaminated plume. However, the plume's extent is larger in the longitudinal (X) direction than in the transverse (Y) direction, which is consistent with the study's assumptions of unidirectional velocity. Moreover, it is evident that the sand bed, located up-gradient of the PRB, accumulates the highest concentrations of contaminants. The greater penetration of the contaminated plume highlights the potential decline in the barrier's effectiveness with increasing flow velocity. In the industry, funnel-and-gate layouts are commonly utilized for PRBs. This design involves placing a permeable gate between two impermeable barriers to direct the contaminated plume into the reactive zone. The concentration distribution is significantly affected by the concentration accumulation at a particular point, and the need to remove higher concentrations as the angle of the impermeable walls increases. Continuous tests proved that the manufactured sorbent can effectively limit the migration of TC front; consequently, it is recommended to apply the present beads in the PRB technology on a field scale.

Sensitivity analysis

The relative significance of the input variables was assessed through sensitivity analysis using the neural network weight matrix and the Garson (1991) equation:

$$I_j = \frac{\sum_{m=1}^{m=Nh}\left(\left(\frac{|W_{jm}^{ih}|}{\sum_{k=1}^{Ni}|W_{km}^{ih}|}\right)\times|W_{mn}^{ho}|\right)}{\sum_{k=1}^{k=Ni}\left\{\sum_{m=1}^{m=Nh}\left(\frac{|W_{km}^{ih}|}{\sum_{k=1}^{Ni}|W_{km}^{ih}|}\right)\times|W_{mn}^{ho}|\right\}} \quad (2)$$

The sensitivity analysis was performed using the neural network weight matrix and the Garson (1991) equation, where Ni and Nh represent the numbers of the input and the hidden neurons, respectively. Ws denotes the connection weights. The superscripts i, h, and o correspond to the input, hidden, and output layers, respectively.

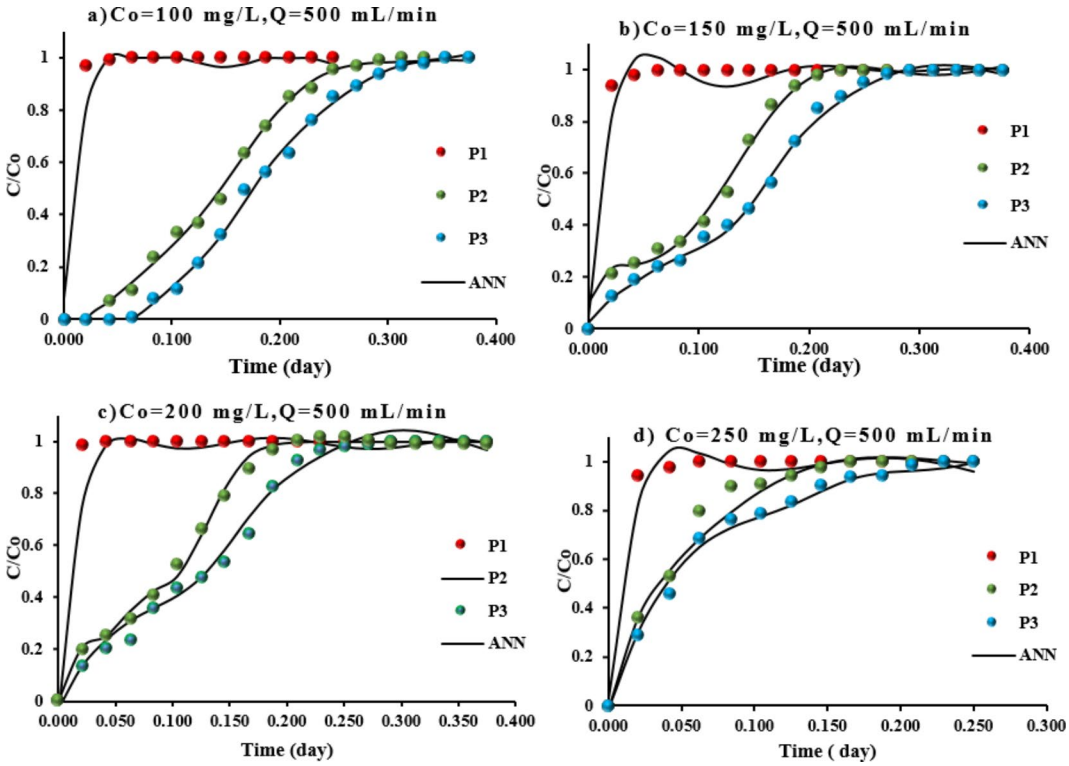

Fig. 15. Comparison between measurements and outcomes of ANN for the sorption of TC onto sodium alginate particles at different ports for flow rate = 500 mL/min, initial concentration = 100,150,200 and 250 mg/L and angle of impermeable walls = 30°.

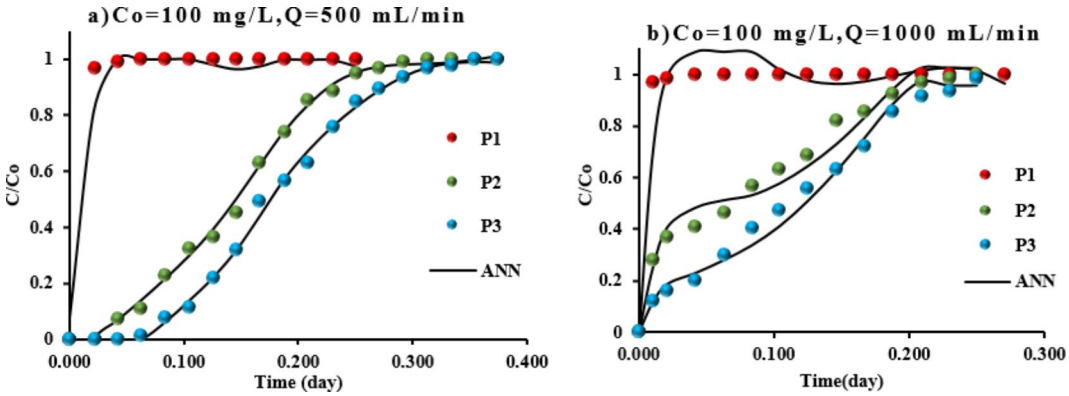

Fig. 16. Comparison between measurements of 2D and outcomes of ANN for the sorption of TC onto sodium alginate particles at different ports for flow rate = 500 and 1000 mL/min, initial concentration = 100 mg/L and angle of impermeable walls = 45°.

The subscripts k, m, and n refer to input, hidden, and output neurons, respectively. The I_j represents the relative importance of the jth input variable on the output variable. The proportional relevance of each input variable is depicted in Fig. 18. It is evident that the flow rate (mL/min) and time (days) have the most significant influence on sorption in the 1D and 2D systems, respectively. However, it is important to note that the range of experimental values used in the model fitting can impact the importance of each variable and its influence on other variables, as demonstrated by several studies.

Conclusions

PRB is an innovative groundwater-cleaning process that is widely used worldwide. The long longevity of the barrier, low operating cost, and hydraulic performance of the barrier have made the in-situ application of PRB quite popular. The outcomes revealed that the optimum parameters for batch experiments were pH 7, contact time 1.5 h, adsorbent dose 1.2 g/50 mL, agitation speed of 200 rpm and initial concentration of TC 100 mg/L,

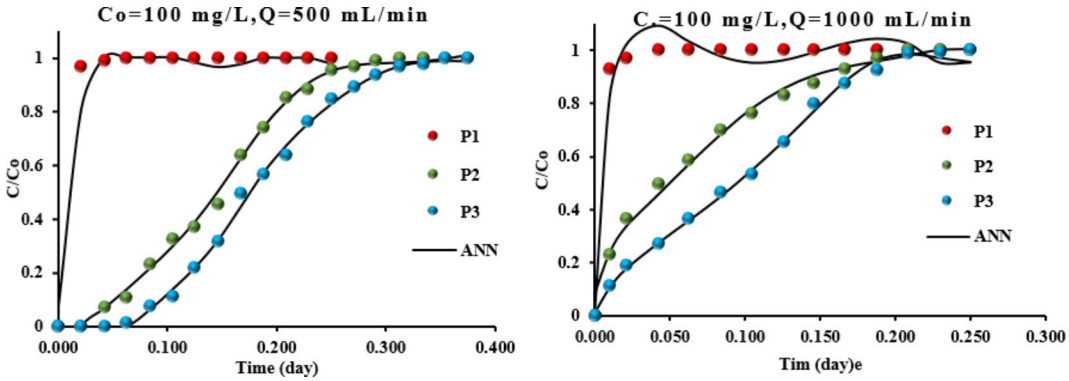

Fig. 17. Comparison between measurements of 2D and outcomes of ANN for the sorption of TC onto sodium alginate particles at different ports for flow rate = 500 and 1000 mL/min, initial concentration = 100 mg/L and angle of impermeable walls = 30°.

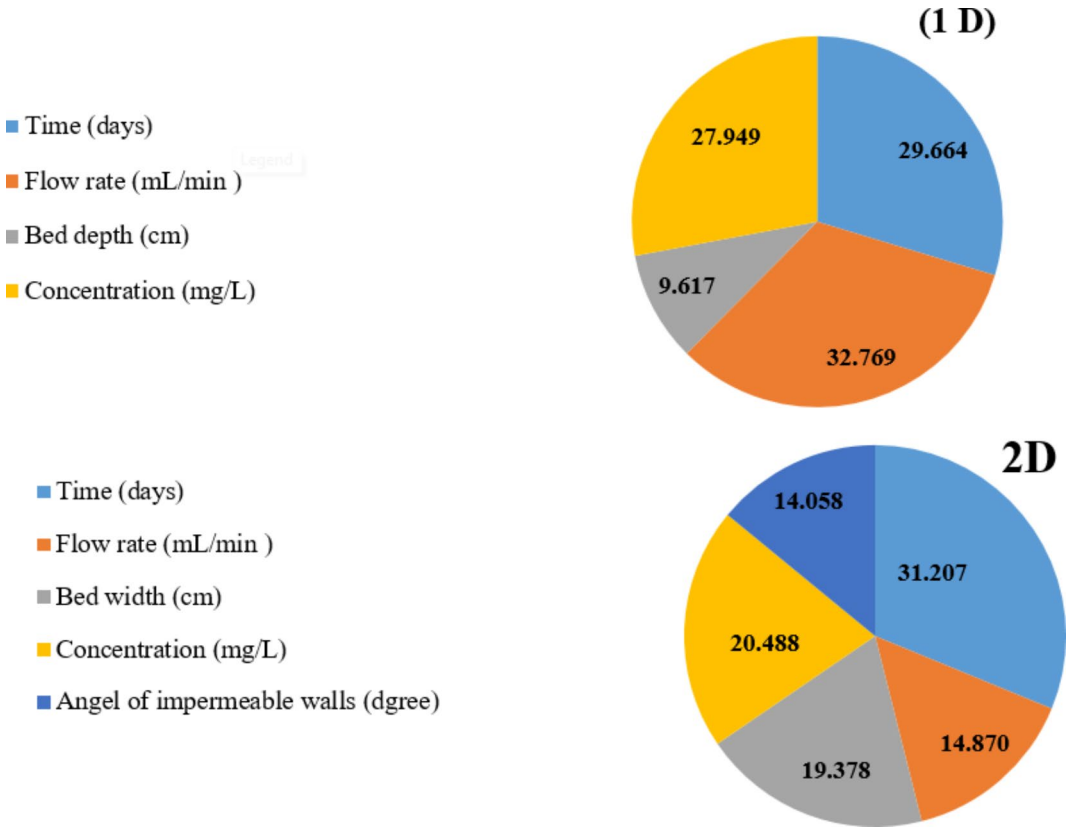

Fig. 18. The sensitivity analysis via the Garson equation and artificial neural network.

which achieved the greatest adsorption capacity (7.845 mg/g) for the interaction of Brownmillerite–Na alginate beads and TC-water. Minimum values of mean square error (MSE) of 7.09E-04 with 30 hidden neurons of 0.0029 with 59 hidden neurons for the 1D network and 2D network, respectively. The artificial neural network model exhibited excellent performance with correlation coefficients exceeding 0.980 for the operating variables, demonstrating its accuracy and effectiveness in predicting the experimental outcomes. According to sensitivity analysis, the influential parameter in the column test (1D) is the flow rate (ml/min), which signifies the relative importance of 32.769%. However, in the tank test (2D), time (day) is signified as an influential parameter with a relative importance of 31.207%. Instead of statistical analysis, mathematical modeling using analytical or numerical solutions for describing contaminant transport through PRB can be a good challenge for future studies, especially since such models are good tools for decision-makers to specify the suitable remedial system.

Data availability

The datasets used and/or analysed during the current study are available from the corresponding author upon reasonable request.

Received: 25 January 2024; Accepted: 16 September 2024
Published online: 02 October 2024

References

1. Kaya, Y. Z. et al. Estimation of daily evapotranspiration in Ko Ice City (Slovakia) using several soft computing techniques. *Theor. Appl. Climatol* **144**, 287–298 (2021).
2. Ogunbanwo, O. M. et al. High concentrations of pharmaceuticals in a Nigerian river catchment. *Environ. Toxicol. Chem.* **41**, 551–558 (2022).
3. valos-Pe a, I. D. et al. Assessment of Physicochemical Groundwater Quality and Hydrogeochemical processes in an area near a municipal landfill site: a case study of the Toluca Valley. *Int. J. Environ. Res. Public. Health* **18**, 11195 (2021).
4. Li, P. & Wu, J. Sustainable living with risks: meeting the challenges, Hum. *Ecol. Risk Assess. Int. J.* **25**, 1–10 (2019).
5. Tiwari, A. K., Singh, A. K. & Mahato, M. K. Assessment of groundwater quality of Pratapgarh district in India for suitability of drinking purpose using water quality index (WQI) and GIS technique, sustain. *Water Resour. Manag.* **4**, 601–616 (2018).
6. Kumar, M. et al. Review of perspective, problems, challenges, and future scenario of metal contamination in the urban environment, *Toxic. Radioact. Waste* **21** 4017007. (2017).
7. Borghi, A. A. & Palma, M. S. A. Tetracycline: production, waste treatment and environmental impact assessment. *Brazilian J. Pharm. Sci.* **50**, 25–40 (2014).
8. Yousefi, M., Farzadkia, M., Mahvi, A. & Kermani, M. Photocatalytic degradation of ciprofloxacin using a novel carbohydrate-based nanocomposite from aqueous solutions, (2024). https://doi.org/10.1016/j.chemosphere.2023.140972
9. Yousefi, M. et al. Comparison of LSSVM and RSM in simulating the removal of ciprofloxacin from aqueous solutions using magnetization of functionalized multi-walled carbon nanotubes: process optimization using GA and RSM techniques. *J. Environ. Chem. Eng.* **9**, 105677 (2021).
10. Naji, A. A. & Abd Ali, Z. T. A single-step method as a green approach to fabricate magnetite nanocomposite for removal of moxifloxacin and cadmium from aqueous solutions. *Environ. Nanatechnol. Monit. Manag* **20**, 100883 (2023).
11. Gopal, G., Alex, S. A., Chandrasekaran, N. & Mukherjee, A. A review on tetracycline removal from aqueous systems by advanced treatment techniques. *RSC Adv.* **10**, 27081–27095 (2020).
12. r Fri t k, V. et al. Pyrogenic materials-Induced immobilization of Eu in aquatic and Soil systems: comparative study. *Water Air Soil. Pollut* **229**, 1–13 (2018).
13. de Ilurdoz, M. S., Sadhwani, J. J. & Reboso, J. V. Antibiotic removal processes from water & wastewater for the protection of the aquatic environment-a review. *J. Water Process. Eng.* **45**, 102474 (2022).
14. Zhang, Y., Zhao, Y. G., Maqbool, F. & Hu, Y. Removal of antibiotics pollutants in wastewater by UV-based advanced oxidation processes: influence of water matrix components, processes optimization and application: a review. *J. Water Process. Eng.* **45**, 102496 (2022).
15. Barbooti, M. M. & Zahraw, S. H. Removal of Amoxicillin from water by adsorption on water treatment residues. *Baghdad Sci. J.* **17**, 1071 (2020).
16. Mokif, L. A. & Faisal, A. A. H. Manufacturing of cost-effective sorbent from by-product materials for treating real and simulated groundwater contaminated with antibiotics. *Desalin. WATER Treat.* **314**, 35–48 (2023).
17. Naushad, M., ALOthman, Z. A., Awual, M. R., Alam, M. M. & Eldesoky, G. E. Adsorption kinetics, isotherms, and thermodynamic studies for the adsorption of pb 2+and hg 2+metal ions from aqueous medium using Ti (IV) iodovanadate cation exchanger. *Ionics (Kiel)* **21**, 2237–2245 (2015).
18. Yang, D. A Review in Tetracycline Removal from Water Environment by Carbon Nanotubes Adsorption, in: IOP Conf. Ser. Earth Environ. Sci., IOP Publishing, : p. 12014. (2021).
19. Ahmad, M. et al. Biochar as a sorbent for contaminant management in soil and water: a review. *Chemosphere* **99**, 19–33. https://doi.org/10.1016/j.chemosphere.2013.10.071 (2014).
20. Premarathna, K. S. D. et al. Clay-biochar composites for sorptive removal of tetracycline antibiotic in aqueous media. *J. Environ. Manage.* **238**, 315–322. https://doi.org/10.1016/j.jenvman.2019.02.069 (2019).
21. Ortiz-Ramos, U., Leyva-Ramos, R., Mendoza-Mendoza, E. & Aragón-Piña, A. Removal of tetracycline from aqueous solutions by adsorption on raw Ca-bentonite. Effect of operating conditions and adsorption mechanism. *Chem. Eng. J.* **432**, 134428. https://doi.org/10.1016/j.cej.2021.134428 (2022).
22. Nodeh, H. R. & Sereshti, H. Synthesis of magnetic graphene oxide doped with strontium titanium trioxide nanoparticles as a nanocomposite for the removal of antibiotics from aqueous media. *RSC Adv.* **6**, 89953–89965 (2016).
23. Graimed, B. H., Abd, Z. T. & Ali Green approach for the synthesis of graphene glass hybrid as a reactive barrier for remediation of groundwater contaminated with lead and tetracycline, Environ. *Nanatechnol. Monit. Manag* **18**, 100685 (2022).
24. Saleem, H. & Zaidi, S. J. Nanoparticles in reverse osmosis membranes for desalination: a state of the art review. *Desalination* **475**, 114171 (2020).
25. Mokif, L. A., Obaid, Z. H. & Juda, S. A. Synthesis of new composite adsorbents for removing heavy metals and dyes from aqueous solution. *J. Ecol. Eng.* **25**, 164–179 (2024).
26. Naji, A. A. & Abd Ali, Z. T. Fabrication of immobilized magnetic nanoparticles for removal of cadmium and moxifloxacin from aqueous solutions using green approach: batch and continuous study, Case Stud. *Chem. Environ. Eng.* 100771. (2024).
27. Lestari, N. D., Nurlaila, R., Muwwaqor, N. F. & Pratapa, S. Synthesis of high-purity zircon, zirconia, and silica nanopowders from local zircon sand. *Ceram. Int.* **45**, 6639–6647 (2019).
28. Cecconet, D., Sabba, F., Devecseri, M., Callegari, A. & Capodaglio, A. G. In situ groundwater remediation with bioelectrochemical systems: a critical review and future perspectives. *Environ. Int.* **137**, 105550 (2020).
29. Antelmi, M., Renoldi, F. & Alberti, L. Analytical and numerical methods for a preliminary assessment of the remediation time of pump and treat systems. *Water (Switzerland)* 12. https://doi.org/10.3390/w12102850 (2020).
30. Painter, B. D. M. Reactive barriers: hydraulic performance and design enhancements. *Ground Water* **42**, 609–617. https://doi.org/10.1111/j.1745-6584.2004.tb02629.x (2004).
31. Kankanige, D. M., Dayanthi, W. K. C. N., Nagasinghe, I. U., Disanayaka, A. M. & Kawamoto, K. Low-cost permeable reactive barrier (PRB) system to treat the Organic compounds and nutrients in the Groundwater contaminated by the landfill-leachate. *Eng. J. Inst. Eng. Sri Lanka* **52**, 15. https://doi.org/10.4038/engineer.v52i2.7350 (2019).
32. Madzin, Z., Kusin, F. M., Zahar, M. S. M. & Muhammad, S. N. Passive in situ remediation using permeable reactive barrier for groundwater treatment. *Pertanika J. Sch. Res. Rev.* **2**, 1–11 (2016).
33. Rad, P. R. & Fazlali, A. Optimization of permeable reactive barrier dimensions and location in groundwater remediation contaminated by landfill pollution. *J. Water Process. Eng.* **35**, 101196. https://doi.org/10.1016/j.jwpe.2020.101196 (2020).
34. Yin, S., Herath, G., Heng, S. & Kalpage, S. Using permeable reactive barriers to Remediate Heavy Metal-Contaminated Groundwater through a Laboratory Column Experiment. *Am. J. Environ. Sci.* **13**, 103–115 https://doi.org/10.3844/ajessp.2017.103.115 (2017).

35. Luo, X. et al. Remediation of arsenic-contaminated groundwater using media-injected permeable reactive barriers with a modified montmorillonite: sand tank studies. *Environ. Sci. Pollut Res.* **23**, 870–877 https://doi.org/10.1007/s11356-015-5254-4 (2016).
36. Wilkin, R. T. et al. Fifteen-year assessment of a permeable reactive barrier for treatment of chromate and trichloroethylene in groundwater. *Sci. Total Environ.* 468–469 https://doi.org/10.1016/j.scitotenv.2013.08.056 (2014).
37. Mokif, L. A. & Faisal, A. A. H. Laboratory studies into Tetracycline removal from aqueous solutions by beads of calcium-Iron oxide nanoparticles. *Water Air Soil. Pollut.* **234**, 1–19 (2023).
38. Naidu, R. & Birke, V. Permeable reactive barrier: Sustainable groundwater remediation, (2014).
39. Mokif, L. A. & Faisal, A. A. H. Funnel and gate permeable reactive barrier permeable reactive barrier configuration for contaminated Groundwater Remediation – Designing, installation, and modeling. *Rev.* **24**, 15–33 (2023).
40. Che Nordin, N. F. et al. Groundwater quality forecasting modelling using artificial intelligence: a review. *Groundw. Sustain. Dev.* **14**, 100643. https://doi.org/10.1016/j.gsd.2021.100643 (2021).
41. Salvo, C. D. Improving Results of Existing Groundwater Numerical Models Using Machine Learning Techniques: A Review, Water (Switzerland). 14 (2022). https://doi.org/10.3390/w14152307
42. Kulisz, M. & Kujawska, J. Application of artificial neural network (ANN) for water quality index (WQI) prediction for the river Warta, Poland. *J. Phys. Conf. Ser.* **2130**https://doi.org/10.1088/1742-6596/2130/1/012028 (2021).
43. Pal, J. & Chakrabarty, D. Assessment of artificial neural network models based on the simulation of groundwater contaminant transport. *Hydrogeol. J.* **28**, 2039–2055 https://doi.org/10.1007/s10040-020-02180-4 (2020).
44. Mohammed, M. A. A., Khleel, N. A. A., Szabó, N. P. & Szűcs, P. Development of Artificial intelligence model with aid of statistical methods for simulation of water quality indices in north Khartoum area. *Sudan. Res. Sq* (2022).
45. Djurovic, N. et al. Comparison of Groundwater Level models based on Artificial neural networks and ANFIS. *Sci. World J.* **2015**https://doi.org/10.1155/2015/742138 (2015).
46. Kulisz, M., Kujawska, J., Przysucha, B. & Cel, W. Forecasting water quality index in groundwater using artificial neural network. *Energies* **14**https://doi.org/10.3390/en14185875 (2021).
47. Al-Waeli, L. K., Sahib, J. H. & Abbas, H. A. ANN-based model to predict groundwater salinity: a case study of West Najaf-Kerbala region. *Open. Eng.* **12**, 120–128 https://doi.org/10.1515/eng-2022-0025 (2022).
48. Ngoie, S., Lunda, J., Mbuyu, A. & Makenda, G. Overview of Artificial neural networks applications in Groundwater studies. *Int. Res. J. Eng. Technol.* 3768–3773. (2018).
49. Golbaz, S., Nabizadeh, R., Rafiee, M. & Yousefi, M. Comparative study of RSM and ANN for multiple target optimisation in coagulation/precipitation process of contaminated waters: mechanism and theory. *Int. J. Environ. Anal. Chem.* **102**, 8519–8537 (2022).
50. Kheradpisheh, Z., Talebi, A., Rafati, L., Ghaneian, M. T. & Ehrampoush, M. H. Groundwater quality assessment using artificial neural network: a case study of Bahabad plain, Yazd, Iran, Desert. **20** 65–71. (2015).
51. Zakeri, H. R., Mohammadi, M. Y. A. A., Mojiri, M. B. S. A. & Hosseinzadeh, S. S. A. Chemical coagulation – electro fenton as a superior combination process for treatment of dairy wastewater: performance and modelling. *Int. J. Environ. Sci. Technol.*https://doi.org/10.1007/s13762-021-03149-w (2021).
52. Groundwater M, Contamination NU (2022) Artificial. Neural Networks Neural Networks -15
53. Khaki, M., Yusoff, I., Islami, N. & Hussin, N. H. Artificial neural network technique for modeling of groundwater level in Langat Basin, Malaysia. *Sains Malaysiana* **45**, 19–28 (2016).
54. Yousefi, M., Esrafili, A., Gholami, M. & Akbar, A. Modeling and analysis of the groundwater hardness variations process using machine learning procedure, **238** 135–141 https://doi.org/10.5004/dwt.2021.27773 (2021)
55. Krishan, L. A. Application of Artificial Neural Network for Groundwater Level Simulation in Amritsar and Gurdaspur districts of Punjab, India. *J. Earth Sci. Clim. Change* **06**https://doi.org/10.4172/2157-7617.1000274 (2015).
56. Di Franco, G. & Santurro, M. Machine learning, artificial neural networks and social research. *Qual. Quant.* **55**, 1007–1025. https://doi.org/10.1007/s11135-020-01037-y (2021).
57. Jia, X. *Field Guide to Hyperspectral/multispectral Image Processing* (SPIE, 2022).
58. Deb, A., Kanmani, M., Debnath, A., Bhowmik, K. L. & Saha, B. Preparation and characterization of magnetic CaFe2O4 nanoparticles for efficient adsorption of toxic Congo Red dye from aqueous solution: predictive modelling by artificial neural network. *Desalin. Water Treat.* 197–209. https://doi.org/10.5004/dwt.2017.21361 (2017).
59. Wang, Y., Gong, S., Li, Y., Li, Z. & Fu, J. Adsorptive removal of tetracycline by sustainable ceramsite substrate from bentonite/red mud/pine sawdust. *Sci. Rep.* **10**, 1–18. https://doi.org/10.1038/s41598-020-59850-2 (2020).
60. Oskoei, V. et al. Removal of humic acid from aqueous solution using UV/ZnO nano-photocatalysis and adsorption. *J. Mol. Liq* **213**, 374–380. https://doi.org/10.1016/j.molliq.2015.07.052 (2016).
61. Faisal, A. A. H. & Naji, L. A. Simulation of ammonia nitrogen removal from simulated wastewater by sorption onto waste foundry sand using artificial neural network. *Assoc. Arab. Univ. J. Eng. Sci.* **26**, 28–34. https://doi.org/10.33261/jaaru.2019.26.1.004 (2019).
62. Ghaemi, M. & Absalan, G. Fast removal and determination of doxycycline in water samples and honey by Fe3O4 magnetic nanoparticles. *J. Iran. Chem. Soc.* **12**, 1–7. https://doi.org/10.1007/s13738-014-0450-6 (2015).
63. Abd Ali, Z. T. et al. Predominant mechanisms for the removal of nickel metal ion from aqueous solution using cement kiln dust. *J. Water Process. Eng.* **33**, 101033. https://doi.org/10.1016/j.jwpe.2019.101033 (2020).
64. Guo, Y. et al. Removal of tetracycline from aqueous solution by MCM-41-zeolite a loaded nano zero valent iron: synthesis, characteristic, adsorption performance and mechanism. *J. Hazard. Mater.* **339**, 22–32. https://doi.org/10.1016/j.jhazmat.2017.06.006 (2017).
65. Phuong, L., Minh, T., Nguyen, P. & Van, H. T. Innovation removal of tetracycline from aqueous solution using composite adsorbent of ZnAl layered double hydroxide and bagasse biochar. *Environ. Technol. Innov.* **28**, 102914. https://doi.org/10.1016/j.eti.2022.102914 (2022).
66. Vu, T. H. et al. Removal of tetracycline from aqueous solution using nanocomposite based on polyanion-modified laterite material, J. Anal. Methods Chem. (2020). (2020).
67. Lu, J., Xu, K., Li, W., Hao, D. & Qiao, L. Removal of tetracycline antibiotics from aqueous solutions using easily regenerable pumice: batch and column study. *Water Qual. Res. J.* **53**, 143–155. https://doi.org/10.2166/wqrj.2018.012 (2018).
68. Abadi, M. H. J., Zhiani, S. M. M. N. R. & Motavalizadehkakhky, H. D. H. A. Removal of tetracycline from aqueous solution using Fe – doped zeolite. *Int. J. Ind. Chem.* **10**, 291–300. https://doi.org/10.1007/s40090-019-0191-6 (2019).
69. Hamoudi, S. A., Hamdi, B. & Brendlé, J. Tetracycline removal from Water by Adsorption on Geomaterial, activated Carbon and Clay Adsorbents. *Ecol. Chem. Eng. S* **28**, 303–328. https://doi.org/10.2478/eces-2021-0021 (2021).
70. Luo, H. et al. E ffi cient Adsorption of Tetracycline from Aqueous Solutions by Modi fi Alginate Beads after the Removal of Cu (II) (2021). https://doi.org/10.1021/acsomega.0c05807
71. Bilas, R., Sriram, K., Maheswari, P. U., Sheriffa, K. M. M. & Begum Highly biocompatible chitosan with super paramagnetic calcium ferrite (CaFe2O4) nanoparticle for the release of ampicillin. *Int. J. Biol. Macromol.* **97**, 513–525. https://doi.org/10.1016/j.ijbiomac.2017.01.036 (2017).
72. Saedi, F. & Hedayati, K. A facile synthesis and study of photocatalytic properties of magnetic CaFe2O4-CeO2 nanocomposites applicable for separation of toxic azo dyes. *J. Nanostruct.* **10**, 497–508. https://doi.org/10.22052/JNS.2020.03.006 (2020).
73. Faisal, A. A. H., Ahmed, D. N., Rezakazemi, M., Sivarajasekar, N. & Sharma, G. Cost-effective composite prepared from sewage sludge waste and cement kiln dust as permeable reactive barrier to remediate simulated groundwater polluted with tetracycline. *J. Environ. Chem. Eng.* **9**, 105194 (2021).

74. Carvalho, I. T. & Santos, L. Antibiotics in the aquatic environments: a review of the European scenario. *Environ. Int.* **94**, 736–757. https://doi.org/10.1016/j.envint.2016.06.025 (2016).
75. Faisal, A. A. H. et al. Green synthesis for novel sorbent of sand coated with (Ca/Al)-layered double hydroxide for the removal of toxic dye from aqueous environment. *J. Environ. Chem. Eng.* **9**, 105342 (2021).
76. Faisal, A. A. H., Al-Wakel, S. F. A., Assi, H. A., Naji, L. A. & Naushad, M. Waterworks sludge-filter sand permeable reactive barrier for removal of toxic lead ions from contaminated groundwater. *J. Water Process. Eng.* **33**, 101112. https://doi.org/10.1016/j.jwpe.2019.101112 (2020).
77. Alshammari, M. et al. Synthesis of a Novel Composite Sorbent coated with Siderite nanoparticles and its Application for Remediation of Water Contaminated with Congo Red Dye. *Int. J. Environ. Res.* **14**, 177–191. https://doi.org/10.1007/s41742-020-00245-6 (2020).
78. Al Juboury, M. F. et al. Synthesis of composite sorbent for the treatment of aqueous solutions contaminated with methylene blue dye. *Water Sci. Technol.* **81**, 1494–1506. https://doi.org/10.2166/wst.2020.241 (2020).

Acknowledgements
We would like gratefully to thank the technical support of the Department of Environmental Engineering at the College of Engineering, the University of Baghdad, Iraq.

Author contributions
Ayad A.H. Faisal wrote Conceptualization, Methodology, Supervision, Validation, Writing – Review & Editing. Layla Abdulkareem Mokif wrote Methodology, Software, Experimental work, and writing.Waqed H. Hassan wrote Visualisation, Review & EditingRadhi AlZubaidi wrote Visualisation, Review & EditingSaeed Al Marri wrote Visualisation, Review & EditingKhalid Hashim wrote Validation, Visualisation, Writing – Review & EditingMohammad Amir Khan wrote Review & EditingOsamah J. Alsareji: Validation, and Review & EditingAll authors reviewed the manuscript.

Declarations

Competing interests
The authors declare no competing interests.

Additional information
Correspondence and requests for materials should be addressed to A.A.F., K.H. or O.J.A.

Reprints and permissions information is available at www.nature.com/reprints.

Publisher's note Springer Nature remains neutral with regard to jurisdictional claims in published maps and institutional affiliations.